Advances in Colloid and Interface Science 276 (2020) 102089

Contents lists available at ScienceDirect

Advances in Colloid and Interface Science

journal homepage: www.elsevier.com/locate/cis

Historical Perspective

Adsorption and interfacial structure of nanocelluloses at fluid interfaces

Pascal Bertsch *, Peter Fischer

Institute of Food Nutrition and Health, ETH, Zurich, 8092 Zurich, Switzerland

ARTICLE INFO

Article history:
17 December 2019
Available online 20 December 2019

Keywords:
Cellulose
Nanocrystals
Nanofibrils
Pickering emulsions & foams
Adsorption
Interfacial structure

ABSTRACT

Nanocelluloses (NCs), more specifically cellulose nanocrystals and nanofibrils, are a green alternative for the stabilization of fluid interfaces. The adsorption of NCs at oil-water interfaces facilitates the formation of stable and biocompatible Pickering emulsions. In contrast, unmodified NCs are not able to stabilize foams. As a consequence, NCs are often hydrophobized by covalent modifications or adsorption of surfactants, allowing also the stabilization of foams or functional inverse, double, and stimuli-responsive emulsions. Although the interfacial stabilization by NCs is readily exploited, the driving force of adsorption and stabilization mechanisms remained long unclear. Here, we summarize the recent advances in the understanding of NC adsorption regarding kinetics, isotherms, and energetic aspects, as well as their interfacial structure, surface coverage, and contact angle. We thereby distinguish unmodified NCs, covalently modified NCs, and surfactant enhanced adsorption.

Contents

1. Introduction

Nanocelluloses (NCs) are obtained by mechanical, enzymatic, or chemical treatment from cellulosic substrates, mostly wood pulp, other plant materials, or bacterial cellulose [1–3]. This yields charged, anisotropic nanoparticles, whereas one distinguishes short rigid cellulose nanocrystals (CNCs), and longer semi-flexible cellulose nanofibrils (CNFs), as visualized in Fig. 1. NCs have attracted attention throughout material sciences due to their biocompatible nature [4], mechanical strength [5], liquid crystal formation [6], or assembly into hydro- and aerogels [7]. In 2011, a new application of NCs was introduced demonstrating their use to stabilize oil-in-water Pickering emulsions [8,9]. This finding has triggered enormous interest and numerous studies have exploited the interfacial stabilization of NCs since as recently reviewed [10,11]. Owed to high steric but also electrostatic

* Corresponding author.
E-mail address: pascal.bertsch@hest.ethz.ch (P. Bertsch).

https://doi.org/10.1016/j.cis.2019.102089
0001-8686/

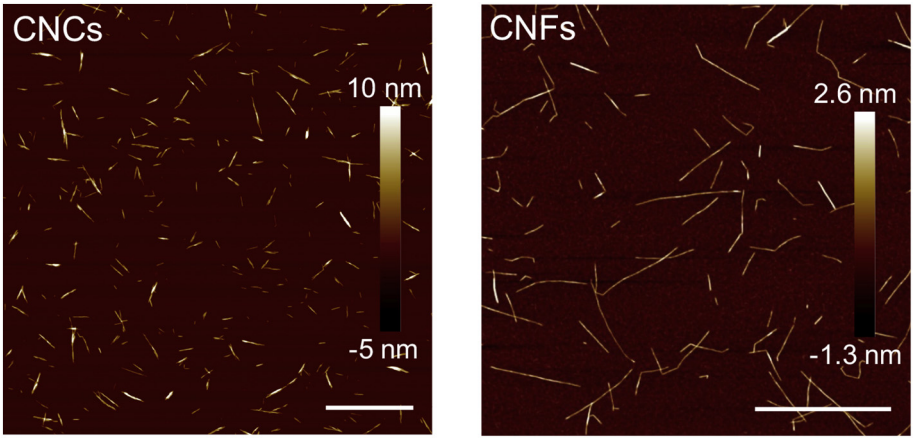

Fig. 1. AFM height images of CNCs and CNFs. The scale bar corresponds to 1 μm. Reproduced with permission from [16,17]. Copyright 2018 and 2019 American Chemical Society.

stabilization, NCs allow the production of emulsions which remain stable for months and resist high temperatures, ionic strengths, altering pH, and even gastric conditions [8,12–15]. Despite successful application, the mechanism of NC adsorption and interfacial stabilization remained long unclear. A key problem was the inability to form controlled NC adsorption layers, the premise of interface sciences, which was recently resolved [16–18]. This has paved the way for the characterization of NC adsorption kinetics and isotherms, as well as structural characterization by displacement and reflectivity techniques. An ongoing enigma is that NCs, while efficiently forming stable emulsions, are not able to stabilize foams [17]. As a consequence, covalent surface modifications or the adsorption of surfactants on the NC surface are exploited to obtain more hydrophobic particles which are able to stabilize foams or reveal desired functionalities [19–22]. These modified NCs however behave substantially different at fluid interfaces. Here, we review the adsorption and interfacial structure of NCs at fluid interfaces, discriminating the three cases of unmodified NCs, covalently hydrophobized NCs, and surfactant enhanced adsorption.

2. Nanocellulose adsorption at fluid-fluid interfaces

NCs may be obtained from a wide range of substrates and production routes, whereas two classes of NCs are distinguished; CNCs and CNFs. CNCs are obtained using acid, mostly sulfuric, to hydrolyze the amorphous regions of cellulose, yielding short rigid nanocrystals 50–300 nm in length with negatively charged sulfate residues [3]. CNFs can be produced by bear mechanical shortening of cellulose fibers [1]. TEMPO-mediated oxidation has emerged as common pretreatment, introducing negative surface charges that facilitate the individualization of fibrils [23]. The mechanical treatment induces defects along the fibril contour; the characteristic kinks [24]. The amount of oxidation agent and intensity of mechanical treatment may be varied to tune the final CNF charge density and length, which usually ranges from a few to several hundred nm [5,25,26]. Hence, both CNCs and CNFs are charged, anisotropic nanoparticles with a considerable aspect ratio, as visualized in Fig. 1. Although NCs have several crystal planes of which some are hydrophobic, they overall behave as primarily hydrophilic particles [3,27,28]. For many applications including interfacial stabilization, more hydrophobic surface properties may be desired, and covalent modifications or adsorption of cationic surfactants thus emerged to alter the surface hydrophobicity of NCs, as schematically illustrated in Fig. 2.

In order to stabilize fluid-fluid interfaces, NCs need to adsorb from the aqueous bulk to the air-water (A/W) or oil-water (O/W) interface. Particle adsorption comprises the diffusion in vicinity to the interface followed by positioning in the liquid-liquid phase boundary [29,30]. The latter is highly dependent on the surface chemistry of the particles, and thus varies for unmodified compared to NCs with hydrophobic surface modifications or adsorbed surfactants.

2.1. Unmodified nanocelluloses

NC adsorption kinetics at a fluid interface were first reported for CNCs at the A/W interface [16] as depicted in Fig. 3A. CNC adsorption curves show a characteristic lag phase followed by adsorption within $\approx$ 15 h, thereby reducing the A/W surface tension γ_{aw} (given as surface pressure $\Pi(t) = \gamma_{aw} - \gamma(t)$). The lag phase around 30–60 min is attributed to a kinetic adsorption barrier and is probably the main reason why the adsorption of unmodified NCs remained long undetected. Adsorption kinetics and Π were enhanced by increasing the CNC bulk concentration up to a saturation at 0.5 wt%. The adsorption of CNCs was further promoted by salt-induced charge screening, as shown in Fig. 3B. The shorter lag phase and faster adsorption suggest that NC surface charges are limiting adsorption, and charge screening decreases the kinetic adsorption barrier. The attained Π from Figs. 3A and B were used to plot adsorption isotherms as a function of CNC and NaCl concentration, as shown in Fig. 3C. The isotherms indicate an increasing surface coverage as a function of CNC bulk concentration with a monolayer saturation at 0.5 wt%. A monolayer structure for NCs is in agreement with imaging and reflectivity methods, as discussed in later sections. Higher Π, and

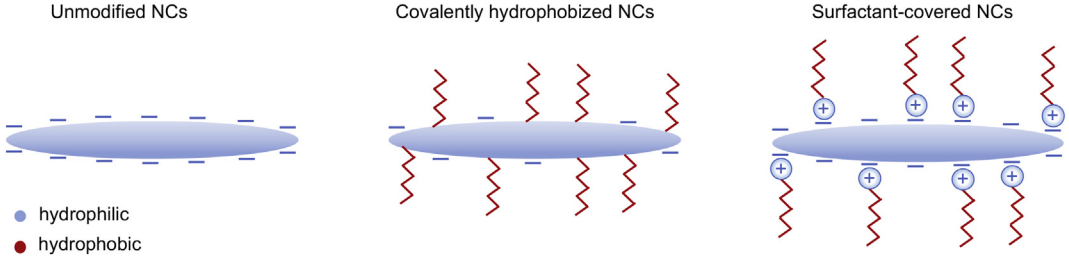

Fig. 2. Schematic illustration of unmodified primarily hydrophilic NCs, NCs with covalent hydrophobic surface modifications, and NCs with adsorbed cationic surfactants.

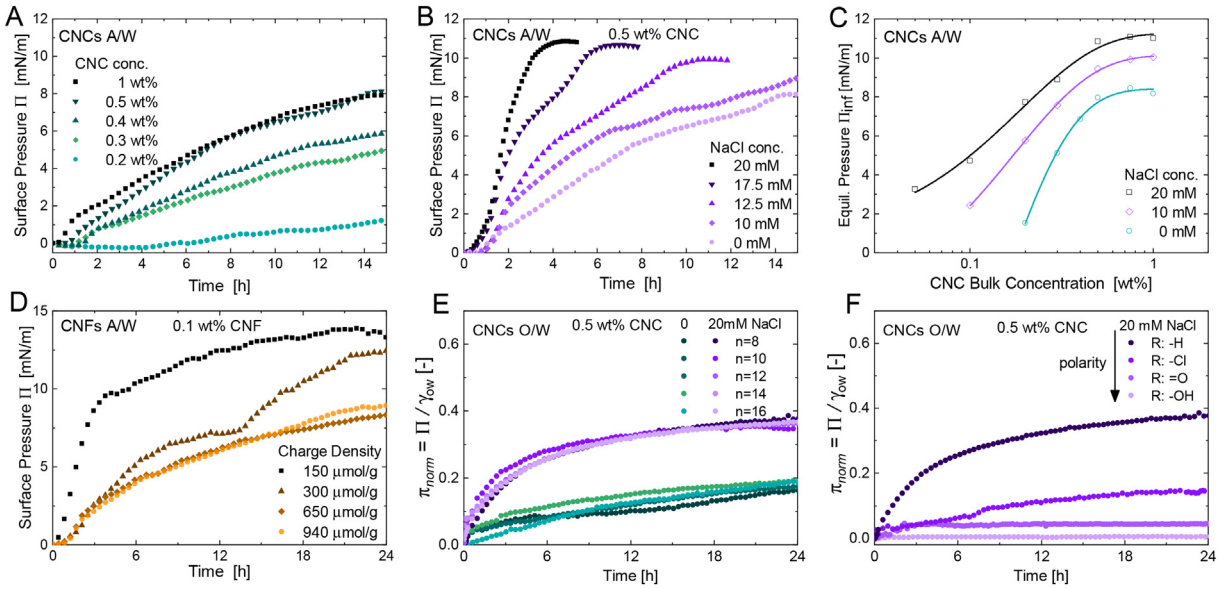

Fig. 3. Compilation of unmodified NC adsorption at fluid interfaces. (A) CNC adsorption at the A/W interface as a function of time for increasing CNC bulk concentration and (B) at 0.5 wt% CNC at increasing NaCl concentration. (C) Adsorption isotherms for CNCs at the A/W interface compiled from the equilibrium surface pressure Π_{inf} from (A) and (B). Adapted with permission from [16]. Copyright 2018 American Chemical Society. (D) Adsorption of CNFs with varying charge density at the A/W interface. Reproduced with permission from [17]. Copyright 2019 American Chemical Society. (E) Adsorption of CNCs at different aliphatic oils with varying chain length from n-octane ($n = 8$) to n-hexadecane ($n = 16$) at 0 and 20 mM NaCl and (F) oils with constant C_8-backbone but increasingly polar headgroup R at 20 mM NaCl. The surface pressure was normalized by the specific O/W interface tension to facilitate comparison within different oils. Reproduced with permission from [18] - published by The Royal Society of Chemistry.

thus coverage, were observed upon charge screening due to lower electrostatic repulsion. Du et al. [31] introduced an area displacement approach that relates the measured Π to the adsorption energy ΔE of an adsorbed nanoparticle:

$$\Pi = -\frac{\Delta E \eta}{A} \quad (1)$$

where η is the covered surface area fraction and A the area covered by one particle. Although Eq. 1 neglects particle interactions and η needs to be determined by another method (see below), this allowed an estimate on the adsorption energy of unmodified NCs. For the employed CNCs, ΔE was in the range of -5 × 10^3 k_BT [16].

A similar adsorption behavior comprising a lag phase and adsorption within ≈ 24 h was reported for CNFs at the A/W interface (Fig. 3D) [17]. Adsorption kinetics and Π were enhanced for CNFs with lower charge density, in agreement with effects of salt-induced charge screening. Hence, NC adsorption can be promoted either by ion-induced charged screening or producing NCs with lower charge density. Varying the length of CNFs had no significant effect on adsorption kinetics and coverage [17]. The CNFs had a very similar ΔE of -7 × 10^3 k_BT according to Eq. 1, as their higher surface area was compensated by a higher coverage.

Bergfreund et al. [18] addressed the adsorption of CNCs at O/W interfaces, as shown in Figs. 3E and F. As for the A/W interface, CNCs adsorbed at the time-scale of hours and adsorption was enhanced by charge screening. No lag phase was apparent at O/W interfaces, potentially due to a more favorable contact angle that prevents the desorption of CNCs and accelerates their net adsorption. Note that profile analysis tensiometry was used to determine CNC adsorption at O/W interfaces, in contrast to the Wilhelmy-plate technique used for A/W interfaces. CNC adsorption at O/W interfaces was independent of the length of aliphatic n-alkanes with constant interface tension γ_{ow} (Fig. 3E). In contrast, CNC adsorption decreased at more polar oils with a lower γ_{ow} (Fig. 3F). This suggests that CNC adsorption is impeded at polar oils with a low γ_{ow} as it results in a lower ΔE [32]:

$$\Delta E = -A\gamma_{ow}(1-|cos\theta|) \quad (2)$$

Altering the oil polarity also changes the contact angle θ of adsorbed NCs, as discussed in detail below. Hence, the positioning and stability of unmodified NCs may vary within oils of different polarity. This finding is quite compelling, considering that the choice of oil is often given little attention in adsorption or emulsion experiments. Bai et al. [14] indeed found differences in droplet size and stability of emulsion formed with different oils. The most polar oil resulted in the largest droplets and least stable emulsions, in good agreement with the impeded adsorption and emulsification reported by Bergfreund et al. [18] This underlines the importance of reporting purification protocols, interface tension, and viscosity of employed oils to allow the comparison within different studies on NC adsorption or emulsions.

The enhanced adsorption at lower charge density or upon charge-screening is attributed to a lower kinetic adsorption barrier. At the clean interface, ion partitioning or image charges may induce electrostatic repulsion and prevent the adsorption of charged particles [33,34]. At increasing particle coverage, the repulsion within particles in the bulk and those adsorbed at the interface increases in importance [35–37]. Pandey et al. [38] demonstrated that CNC adsorption may also be triggered by higher salt concentrations that induce colloidal instability, resulting in higher surface coverage. Besides impeding adsorption, surface charges seem to limit the maximum Π and thus NC surface coverage. It is not entirely clear whether this derives from the higher kinetic adsorption barrier or repulsive capillary forces that arise within adsorbed particles [39]. These findings of charge limited adsorption are in good agreement with findings from emulsion, where NCs fail to stabilize emulsions beyond a critical charge density [38,40]. In contrast to surface charges, varying the length L of CNFs had no significant effect on adsorption kinetics and surface pressure [17], although the excluded area of an adsorbed particle scales ~ L^2 and is significantly larger than its Debye length [24,41]. A possible reason is that the excluded area is outplayed by attractive capillary forces which arise within anisotropic particles due to quadrupolar interface distortions [42,43]. Faster adsorption compared to CNCs was reported for nanocrystals extracted from holocellulose, which was attributed to remains of lignin which is more hydrophobic than NCs [44–46].

Besides A/W and O/W interfaces, CNCs have also been demonstrated to stabilize *W*/W emulsions in presence of two incompatible hydrophilic polymers [47,48]. This is promising as the interface in W/W emulsions is several nm thick and cannot be stabilized by surfactants.

As indicated above, the adsorption of NCs at fluid interfaces remained long undetected, leaving many aspects of NC interfacial stabilization unexplained. For instance, it was not clear whether unmodified NCs induce a reduction in interface tension. The findings summarized in this section demonstrate that unmodified NCs adsorb within hours and reduce the A/W or O/W interface tension. Note that the slow adsorption in diffusion limited experiments is no contradiction to the efficient emulsion stabilization by NCs, as high shear forces during emulsification outplay diffusion and kinetic adsorption barriers. It was also unclear if NCs behave as amphiphilic particles at fluid interfaces, considering that they have primarily hydrophilic and hydrophobic crystal planes [27,28]. Their slow net adsorption and dependence on oil polarity support that they behave as primarily hydrophilic particles, in agreement with their behavior in bulk [3,27]. Li et al. [49] confirmed that CNCs with a more hydrophobic crystalline allomorph are more efficient emulsion stabilizers. The effect of NC surface chemistry on adsorption behavior will be evident in the following sections addressing NCs with surface modifications or adsorbed surfactants, yielding NCs with higher hydrophobicity and lower surface charge.

2.2. Covalently hydrophobized nanocelluloses

Besides the use of native NCs, their surface may be chemically modified to obtain more hydrophobic particles [3,50]. The most common covalent modifications for interfacial stabilization comprise short methyl [51–54], ethyl [20,54–59], or acetyl groups [60], silylation [9,61,62], esterification with longer alkyls [63–69], or polymer grafting [70–80]. The resulting hydrophobic NCs behave substantially different at fluid interfaces compared to unmodified NCs.

Bizmark et al. performed a series of systematic studies on the adsorption of ethylated CNCs at the A/W and O/W interface [57–59]. Ethylated CNCs adsorb already after a few seconds and reduce the interface tension by 30 mN/m, as shown in Figs. 4A, B, and C. This is in strong contrast to the adsorption of unmodified CNCs shown in Figs. 3A and B, where a lag phase of 30–60 min was observed at tenfold higher concentrations and the surface tension was reduced by no more than 10–15 mN/m. The higher Π suggests a significantly higher coverage in case of modified NCs, i.e. their Gibbs surface excess is increased due to their hydrophobicity. In fact, the authors could confirm that close packing is likely. Using Eq. 1, this resulted in a ΔE of ≈ -5 × 10^4 k_BT for esterified CNCs [58,59], one order of magnitude higher than reported for unmodified NCs [16–18]. As the exact surface coverage could not be determined experimentally the authors assumed hexagonal close packing for spherical particles ($\eta = 0.91$).

Bizmark et al. [57–59] further observed that the adsorption of ethylated CNCs is barrierless, i.e. only limited by diffusion, again in contrast to unmodified NCs which are limited by a charge induced kinetic adsorption barrier. Interestingly, the zeta-potential of ethylated CNCs was −60 mV and DLVO theory thus suggested the presence of a charge barrier. The authors could attribute this discrepancy to a hydrophobic attraction force within the ethylated CNCs that facilitates barrierless adsorption at the interface without inducing aggregation in bulk. The absence of a charge induced kinetic adsorption barrier was confirmed by salt addition, which had no effect on adsorption as shown in Fig. 4B.

A direct comparison of hydrophobized CNCs grafted with PIIP (poly[2-isopropoxy-2-oxo-1,3,2-dioxaphospholane]) and unmodified CNCs was presented by Hiranphinyophat et al. [77], as depicted in Fig. 4D. The modified CNCs again reduced the interface tension by ≈ 30 mN/m already at 0.1 wt%, whereas no changes were observed for unmodified CNCs at this concentration. The unmodified CNCs reduced the surface tension by 10 mN/m at 0.4 wt%, in good agreement with the adsorption isotherm previously shown in Fig. 3C. Scheuble et al. [51,53] also found Π ≈ 30 mN/m already at 0.01 wt% for methylated CNCs (Fig. 4E). Moreover, methylated CNCs were able to replace a previously adsorbed layer of the protein β-lactoglobulin, a behavior commonly observed for surfactants [81]. Unmodified CNCs on the other hand did not induce changes in surface tension at these concentrations and did not replace the adsorbed protein, but instead formed a secondary layer

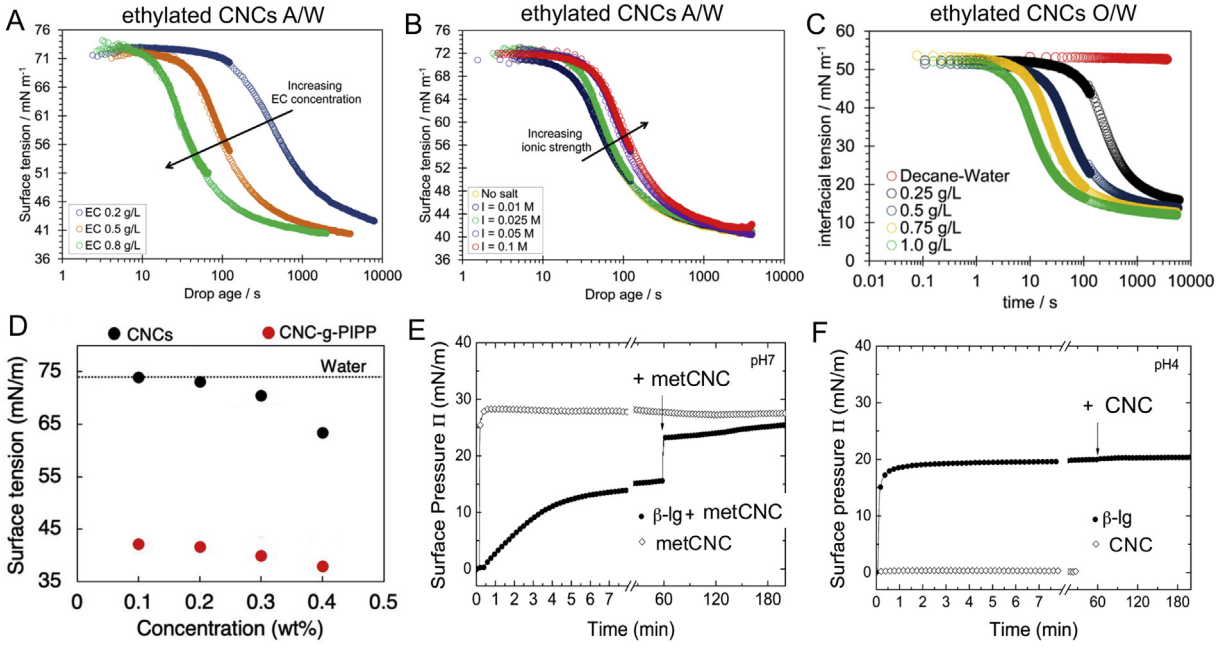

Fig. 4. Compilation of modified NC adsorption at fluid interfaces. Surface tension as a function of time for ethylated CNC (ethCNC) adsorption at (A) the A/W interface at increasing ethCNC concentration, (B) varying ionic strength, and (C) the O/W interface at increasing ethCNC concentration. Reprinted with permission from [58,59]. Copyright 2015 and 2017 American Chemical Society. (D) Adsorption isotherms of unmodified CNCs in comparison to CNCs grafted with poly[2-isopropoxy-2-oxo-1,3,2-dioxaphospholane] (CNC-g-PIPP). Adapted with permission from [77]. Copyright 2019 American Chemical Society. (E) Surface pressure as a function of time for methylated CNCs (metCNC) and the whey protein β-lactoglobulin (β-lg) followed by metCNC addition, demonstrating the displacement of β-lg by metCNC. (F) Adsorption of cationic β-lg (pH 4) followed by the addition of unmodified anionic CNCs, resulting in an electrostatically complexed multilayer. Adapted with permission from [51]. Copyright 2014 American Chemical Society.

bound electrostatically (at pH 4) to the primary protein layer (Fig. 4F). The double layer structure was confirmed by neutron reflectometry as discussed below.

Hence, NCs with hydrophobic surface modifications adsorb significantly faster and reach lower surface tensions, and thus higher surface coverage. However, as unmodified NCs efficiently stabilize O/W interfaces during emulsification, this is generally not the motivation for their hydrophobization. Surface modifications can be exploited to create NCs with desired functionalities for various applications. Most importantly, unmodified NCs are not able to stabilize foams despite the reduction in surfacetension discussed above. This probably derives from an unfavorable contact angle of unmodified NCs at the A/W interface [17,18], as discussed in detail below. In contrast, hydrophobized NCs can be used to form stable foams [20,55,56]. An alternative for the production of cellulose stabilized foams was presented by Rühs et al. [82], who produced a foam containing *Gluconoacetobacter xylinus* which formed bacterial cellulose directly at the A/W interface. Zhang et al. [83] demonstrated the formation of stable nanoemulsions using modified NCs. Nanoemulsions can also be obtained with unmodified NCs, but are more energy intensive and require multiple steps [84]. Another motive is the production of inverse W/O emulsions. Whereas NCs modified with short alkyl or carboxyl groups still form O/W emulsions [59,73,85], an inversion is observed for more hydrophobic NCs modified with longer fatty acids or polymers [9,63,68,86–88]. The formation of inverse emulsions suggests that these particles are primarily wetted by the oil phase, which is not possible for unmodified NCs even for polar oils [18]. This is underlined by studies investigating CNCs modified with alkyls with increasing length, which resulted in a higher affinity towards the oil phase [83,87]. Other studies investigated NCs with increasing degree of substitution (DS) with hydrophobic moieties, confirming that the contact angle of CNCs is shifted towards the hydrophobic subphase at higher DS [65,66,80,88]. Hence, increasing the NC hydrophobicity results in a higher contact angle, allowing the production of inverse W/O emulsions beyond a critical hydrophobicity. The combination of such modified NCs and unmodified NCs can be exploited for the production of double W/O/W emulsions [63].

NC surface modifications may also be exploited to form stimuli-responsive emulsions. Methylated CNCs form a monolayer at the O/W interface at room temperature which gels into a thick multilayer upon heating to 37°C [52,53]. This thermogelation at body temperature was proposed for gastric stable emulsions that gel in the stomach and form indigestible interfacial layers. Other examples are pH [89] or magnetically responsive emulsions [90]. Polymer grafting is probably the most promising route to produce responsive emulsions owed to the wide range of polymers available [91]. Polymer grafted NCs can be used to stabilize emulsions which break above the lower critical solution temperature of the polymers [70–72,74,77]. Glasing et al. [78] used a CO_2-sensitive polymer to form emulsions which break and re-emulsify upon sparging with CO_2 and N_2, respectively. Polymers with pH-dependent charge were employed for emulsions which are stable in a given pH-range [74,75,79]. Note that unmodified NCs may also reveal different pH-responsiveness depending on the nature and density of their surface charges [92,93]. An interesting modification, although resulting NCs are not more hydrophobic, are magnetic Fe-modified NCs investigated by Low et al. [94–97]. The Fe-modified NCs form Pickering emulsions which can be destabilized at will by an external magnetic field, which was employed to trigger the release of encapsulated bioactive compounds for drug delivery applications [95]. Resulting emulsions are also pH-responsive due to the pH-dependent solubility of Fe-modified NCs [96,97].

2.3. Surfactant enhanced adsorption

Besides covalent surface modifications, the surface chemistry of NCs can be altered by the adsorption of other surface-active species. Most commonly, cationic surfactants are used that assemble at the anionic NC surface with their alkyl chains oriented towards the aqueous phase, resulting in hydrophobic NC-surfactant aggregates [19,21,22,98–101]. The adsorption of cationic surfactants depends on the NC surface charge and presence of counterions, and may induce a positive charge inversion of the aggregates [102]. The motivation for surfactant adsorption on the NC surface is essentially the same as for covalent modifications discussed above; surfactant-covered NCs are more hydrophobic allowing for lower surface tension and higher surface coverage [19,21,99,101], formation of stable foams [22,98], or inverse and multiple emulsions [99,103].

Hu et al. [99] investigated the effect of didecyldimethylammonium bromide (DMAB) on CNC adsorption at the A/W and O/W interface. The interface tension was higher in presence of CNCs compared to DMAB only (Fig. 5A and B). Hence, the presence of CNCs impeded the surfactant surface coverage. The opposite effect was reported for other

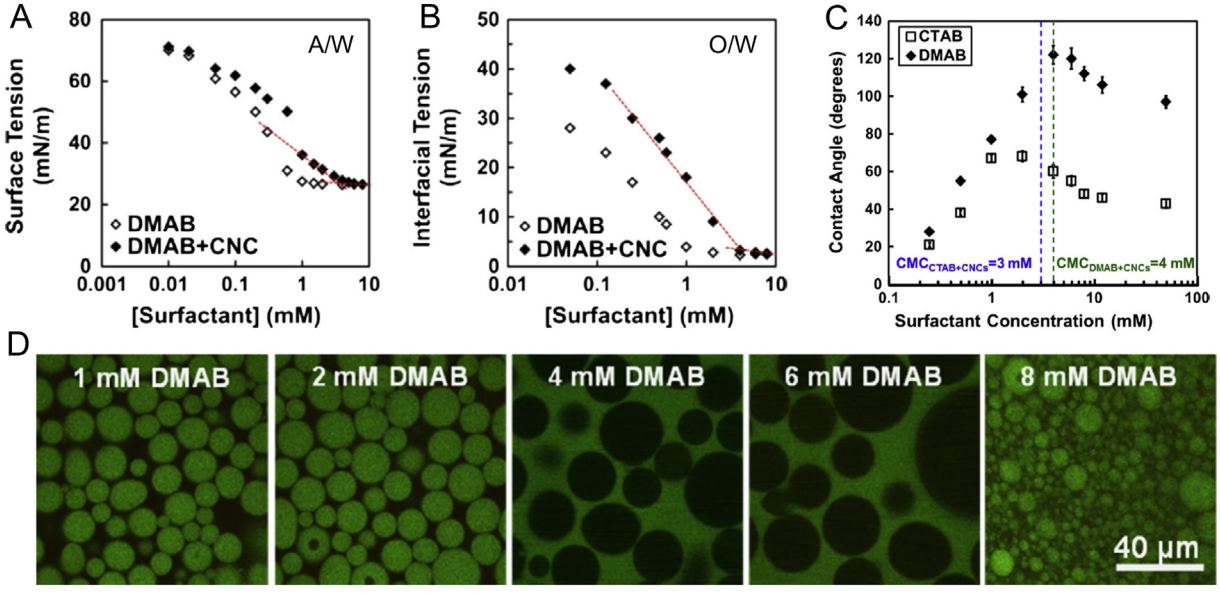

Fig. 5. Interfacial tension as a function of DMAB concentration in absence and presence of CNCs at the (A) A/W and (B) O/W interface. (C) The hydrophobicity of CNCs at increasing amount of adsorbed DMAB and CTAB expressed by the contact angle of surfactant solutions on CNC films showing maximum hydrophobicity around the CMC. (D) Confocal laser scanning micrographs of 1:1 water/dodecane emulsions (the dodecane was dyed green) stabilized by CNCs with increasing amount of DMAB showing a phase inversion at 4–6 mM, in agreement with the maximum hydrophobicity displayed in (C). Reprinted from [99]. Copyright Elsevier 2015.

surfactants [19,21,104], suggesting that synergistic effects may also be possible. Hu et al. [99] further investigated the hydrophobicity of CNCs at increasing surfactant concentrations, as shown in Fig. 5C. The hydrophobicity of NCs initially increases due to the adsorption of surfactants, but is eventually inverted close to the critical micelle concentration (CMC), indicating the formation of surfactant multilayers. This alternating hydrophobicity was exploited for the formation of inverse W/O emulsions close to the CMC where the NCs show maximum hydrophobicity, whereas O/W emulsions were formed below or above the CMC (Fig. 5D). No phase inversion was possible with the less hydrophobic surfactant cetyltrimethylammonium bromide (CTAB), nicely demonstrating that the NC-surfactant complexes need to exceed a critical hydrophobicity and be primarily wettable by the oil phase to form inverse emulsions. Most studies have addressed surfactant concentrations $\pm$ 2 decades around the CMC. However, Anyfantakis et al. [105] demonstrated that surfactants promote the adsorption of counter-charged nanoparticles already at concentrations thousandfold below their CMC, although they do not significantly alter the hydrophobicity nor zeta-potential at these concentrations. An elegant application for surfactant-induced NC adsorption was demonstrated by Reid et al. [106]. The adsorption of NCs at an O/W interface was triggered by the addition of cationic aromatic diamines. Acyl chloride was dissolved in the oil phase which polymerized with the diamines upon adsorption, allowing the formation of nanocomposite films, fibers, and spheres whose surface properties are dominated by the NCs which form the outermost layer.

Besides the formation of NC-surfactant aggregates in the bulk to modify NC hydrophobicity, cationic surfactants may be dissolved in the oil. The surfactants adsorb at the O/W interface and expose their cationic headgroup to the aqueous bulk, thereby promoting the adsorption of anionic NCs. The main advantage of this approach is that NC adsorption can be tuned by the NC and surfactant charge. For instance, surfactants with pH-dependent charge were used for the formation of interfacial layers where the coverage and surface tension could be controlled by pH [107–109]. Calabrese et al. [110] demonstrated that the adsorption of CNFs at an O/W interface loaded with cationic oleylamine can be modulated via ionic strength. An interesting application was presented by Kaufman et al. [111], who employed microfluidics to produce elastic microcapsules by the interfacial complexation of CNFs and a cationic oil-soluble copolymer.

Remains the question if NC adsorption may also be enhanced by nonionic or even anionic surfactants. Anionic and nonionic surfactants have been given little attention as they adsorb at the less charged regions of NCs by hydrophobic interactions, thereby not altering NC hydrophobicity [112]. When adsorbed at the liquid-liquid interface, these surfactants expose their hydrophilic moieties towards the aqueous phase, which is not expected to promote NC adsorption. Hence, it is questionable if non- and anionic surfactants can promote NC adsorption. Wu et al. [109] employed an oil-soluble cationic surfactant with pH-dependent charge, revealing a significantly lower CNC coverage at decreasing surfactant charge. Nevertheless, it was demonstrated that the combination of nonionic alkyl polyglucoside and NCs result in emulsions with smaller droplet size and prolonged stability compared to employing them individually [104]. Similar results were reported by Xiang et al. [113] for foams stabilized by a combination of anionic sodium dodecyl sulfate and CNFs. The addition of CNFs enhanced foam stability compared to the pure surfactant foams, which was attributed to an increase in bulk and interfacial elasticity by CNFs. On the other hand, a study investigating emulsification in high ionic strength brines reported adverse effects of combining NCs with nonionic surfactants, while confirming synergistic effects of cationic surfactants [114]. The nonionic surfactants adsorbed on the NCs and the complexes did not adsorb, thereby limiting the amount of surfactants available for interfacial stabilization. Hence, the role of non- and anionic surfactants on CNC adsorption remains ambiguous. A general problem in such investigations is that the employed surfactants reduce the surface tension themselves, making it difficult to distinguish the actual adsorption of NCs. A possible approach is the use of interfacial shear rheology which facilitates the measurement of NC adsorption via interfacial viscoelasticity independent of surface tension [110].

NCs can also be combined with other surface active species to form interfacial composites. Similar to surfactants, cationic proteins can be used to alter the hydrophobicity of NCs and promote their adsorption [115,116]. Scheuble etal. [51,53] introduced the formation of a primary cationic protein layer followed by electrostatic complexation of anionic CNCs, resulting in interfacial double layers. The CNCs sterically protected the protein layer from proteases, yielding gastric stable adsorption layers. The concept was later confirmed to result in invitro gastric stable emulsions [117]. Hu etal. [118,119] combined NCs with larger, surface active cellulose derivatives (ethyl, methyl, or hydroxyethyl cellulose) which resulted in smaller emulsion droplets and allowed the formation of stable foams. Bielejewska and Hertmanowski [120] demonstrated that CNCs adsorb at previously established interfacial liquid crystal layers. The authors could obtain CNC-liquid crystal composites with improved stability and mechanical properties. Such composites with the electro- and thermo-optical properties of liquid crystals and the mechanical features of CNCs were proposed for flexible or shape-adaptive sensors and display elements.

3. Interfacial layer structure, surface coverage, and contact angle

The structure, surface coverage, and particle positioning at a fluid interface can ultimately affect the stability of the individual particles and resulting colloidal materials. These parameters may vary significantly for unmodified, modified, or surfactant-induced NC adsorption, as discussed in the previous section. The structural analysis of adsorbed particles in the nano-range is not straightforward, and related methods are often invasive or limited to qualitative statements. Nevertheless, the insights from scanning electron microscopy (SEM), interfacial displacement techniques, and interfacial reflectometry complement each other and, if combined, provide a decent understanding of NC interfacial layer structure.

3.1. Structure and coverage in nanocellulose stabilized emulsions and foams

When Kalashnikova etal. [8] first reported on the emulsion stabilization by bacterial cellulose, they were confronted with the problem that the oil (hexadecane) would evaporate during preparation for SEM experiments. As a workaround, styrene/water emulsions with comparable interface tension and droplet size were prepared, followed by the polymerization of styrene overnight. The solidified polystyrene with adsorbed bacterial cellulose could be imaged by SEM, showing a densely packed interfacial network with overlapping CNFs that form interconnected droplets (Fig. 6A). The same technique was later used to image shorter CNCs [121], showing a smoother CNC monolayer with CNCs being too short to interconnect the droplets (Fig. 6B). The protrusion of CNFs into the bulk and formation of interconnected networks are considered to provide additional stabilization [84]. The combination of densely adsorbed CNCs and additional bulk thickening by CNFs was recently exploited by Bai et al. [122] An alternative allowing visualization with the actual oil is freeze fracture cryo-SEM, allowing the imaging of craters left by emulsion droplets with adsorbed CNCs in the fracture plane (Fig. 6C) [13,38]. This technique was also used by Jin et al. [56] to image air bubbles in foams stabilized by ethylated cellulose (Fig. 6D). In contrast to unmodified CNCs, ethylated cellulose formed rough multilayers due to particle aggregation at the interface. Further, confocal or fluorescence microscopy may be employed to visualize the structure and distribution of NCs in multiphase systems [8,12,38,47,63,113].

The main drawback of emulsion imaging is that only qualitative information is obtained. Complementary, the surface coverage η may be quantitatively approximated in the limited coalescence regime (lowest

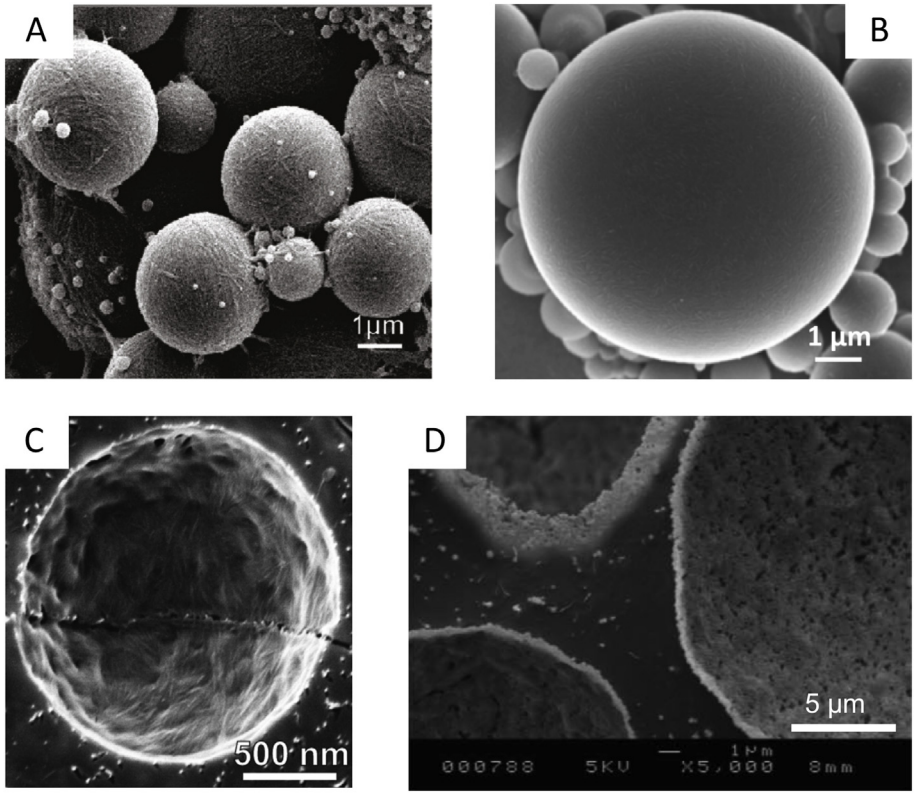

Fig. 6. SEM images of NC stabilized emulsions and foams. (A) CNFs and (B) CNCs adsorbed in polymerized polystyrene/water emulsions. Reprinted with permission from [8,121]. Copyright American Chemical Society 2011 and 2015. The crater left by (C) a CNC stabilized MCT-oil/water emulsion droplet and (D) air bubbles in ethylated cellulose stabilized foams after freeze fracturing. (C) Reprinted with permission from [13]. Copyright American Chemical Society 2018. (D) Reprinted from [56] - published by The Royal Society of Chemistry.

NC concentrations facilitating stable emulsions) by the emulsified oil volume V_{oil} and the mean droplet diameter D [8]:

$$\eta = \frac{mD}{6h\rho V_{oil}} \tag{3}$$

where m, h, and ρ are the mass, height, and density of the used NC. This approach compares the total oil surface that needs to be stabilized to the surface area of NCs that is in contact with oil, assuming the NCs adsorb as flat rectangles. The mass m is corrected by the remaining NCs in the aqueous supernatant after centrifugation which has not adsorbed at the interface, which however is usually negligible in the limited coalescence regime [8]. This approach revealed that short CNCs form a dense interfacial network with up to 80% surface coverage, whereas longer CNFs with higher aspect ratio form more loose layers and stabilize emulsions already at 45% coverage [123]. A possible explanation for the higher coverage of CNCs is their straight morphology that eases packing compared to the kinked and semi-flexible CNFs [124]. The same approach was employed by Peddireddy et al. [47] for *W*/W emulsions, revealing a surface coverage of 50% for CNCs. The droplet diameter in O/W emulsions is generally around 4 μm independent of NC length. In contrast, the emulsion droplet size increases for NCs with higher charge density, and no emulsions can be formed beyond a critical charge density of 0.03 e/nm^2 [40]. Surface charges can limit the adsorption and coverage of NCs due to a higher kinetic adsorption barrier and repulsive capillary interactions, as discussed above (Fig. 3). The coverage observed in emulsions is generally higher than those reported for 2D interfacial layers (20–40% [16,17]). It is thus suggested that the interface tension reduction of NCs in emulsions exceeds the 10–15 mN/m discussed above (Fig. 3).

The most detailed structural analysis of NC stabilized emulsions was provided by Cherhal et al. [121] using small-angle neutron scattering (SANS) with additional contrast variation. The scattering length density of the subphases was altered using different ratios of deuterated water and oil (hexadecane) to probe the structure of the adsorbed CNC layer. The thickness of the CNC layer was 7 nm, equal to the height of one CNC which confirmed previous speculations that NCs form monolayers. In contrast, when the CNCs were desulfated and were no longer charged, they formed lose aggregates 18 nm in thickness. Pandey et al. [38] confirmed that thicker layers are formed from desulfated CNCs by electron and confocal microscopy. Thus, it appears that the surface charges limit the layer thickness to a monolayer. The contrast variation further allowed first insights on CNC positioning and contact angle at the O/W interface. Interestingly, the CNCs remained mostly in the aqueous phase. It was concluded that the CNCs are only in contact with the oil by the most hydrophobic (200) crystal plane. This is surprising considering that a contact angle < 90° is energetically unfavorable and seems to be in contradiction to the high stability and irreversible adsorption observed for NCs adsorbed at O/W interfaces. The discussion on NC contact angle and implications on emulsion and foam stability is continued in a later section.

3.2. Structure analysis of 2D adsorption layers

Although 2D adsorption layers may appear substantially different from the adsorption in foams and emulsions, they offer many advantages for structure analyses. Film displacement by the Langmuir-Blodgett or Langmuir-Schaefer technique has revealed significant differences in the structure of adsorbed NC layers depending on their modification, which are difficult to observe in emulsions. The rather invasive film displacement may be complemented with non-invasive interfacial reflectivity measurements. Finally, the viscoelastic properties of 2D adsorption layers may be assessed using interfacial shear or dilatational rheology, linking the observed structure to a specific mechanical response.

3.2.1. Displacement and imaging of nanocellulose adsorption layers

The first reports on NC interfacial film displacement and imaging date back to 2007, several years before NCs received attention for the stabilization of fluid interfaces. Habibi et al. [19,126] used a cationic surfactant to induce CNC and CNF adsorption at the A/W interface followed by Langmuir-Blodgett displacement, aiming at the production of crystalline cellulose surfaces. The formation of unmodified NC adsorption layers was addressed more recently [16], allowing their displacement and imaging as shown in Fig. 7A. The unmodified CNCs formed a lose monolayer with a surface coverage of 20%. The CNCs did not aggregate which was attributed to electrostatic repulsion. No signs of preferential orientation were observed, probably due to the low surface coverage. In contrast, Habibi et al. [19] found a densely covered monolayer for surfactant-induced CNF adsorption (Fig. 7B). The preferred orientation of the fibers was initially attributed to the directed extraction of the substrate. However, their later work suggested that NCs may in fact form ordered 2D liquid crystalline phases beyond a critical surface load [126].

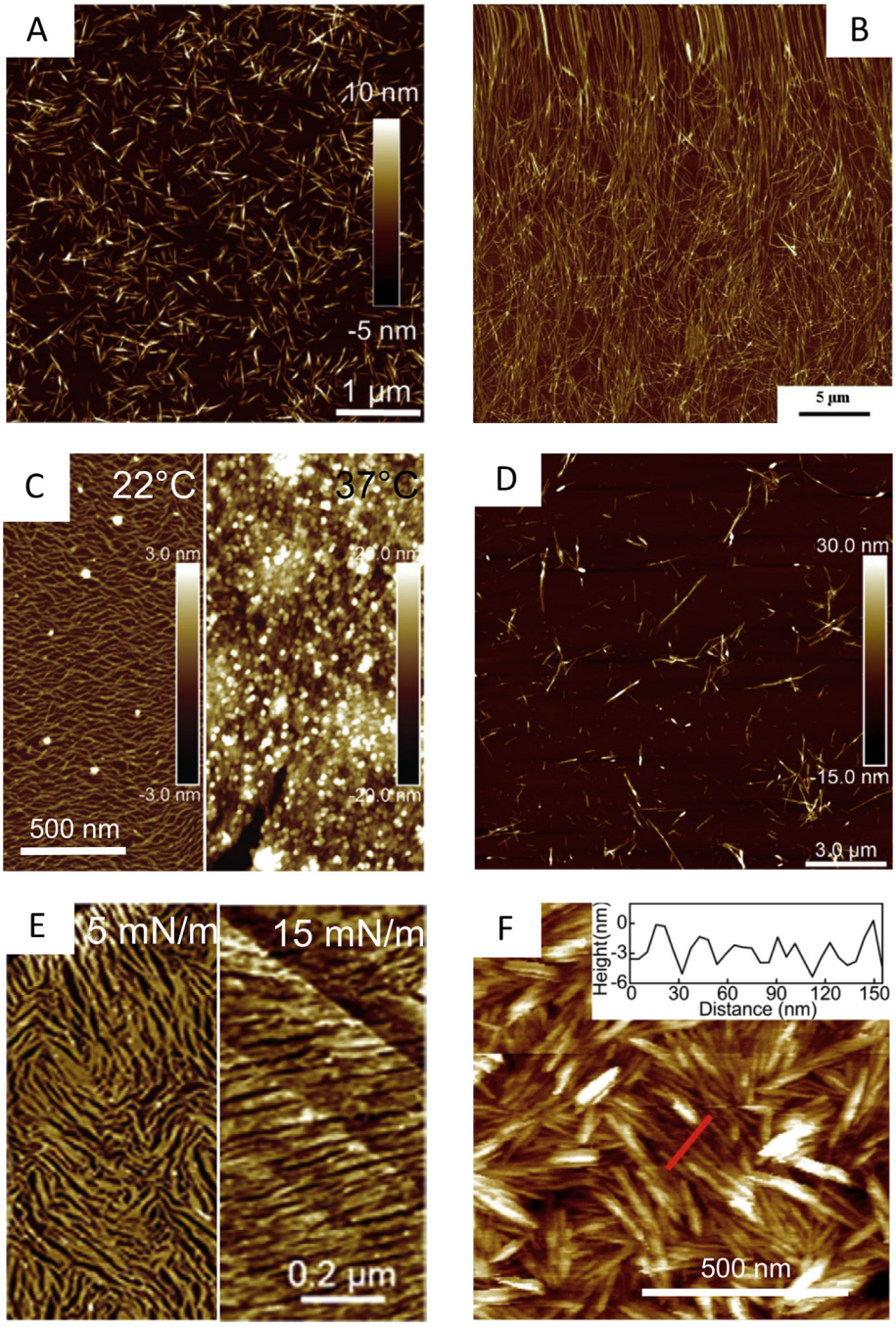

Fig. 7. Compilation of different interfacial structures obtained for unmodified, modified, and surfactant-induced NC layers. AFM height images of interfacial layers displaced from the A/W interface of (A) unmodified CNCs. Reprinted with permission from [16]. Copyright 2018 American Chemical Society. (B) CNFs adsorbed with a cationic surfactant (DODA) followed by washing out DODA using chloroform. Reprinted with permission from [19]. Copyright Elsevier 2007. (C) Methylated CNCs at 22°C and after thermogelation at 37°C. Reprinted with permission from [52]. Copyright 2016 American Chemical Society. (D) CNCs esterified with C_{16} alkyl groups. Reprinted with permission from [65]. Copyright 2018 American Chemical Society. (E) Cellulose triacetate transferred on a hydrophobic substrate (HOPG) at different surface pressures. Reprinted with permission from [125]. Copyright Elsevier 2015. (F) In situ liquid AFM of CNCs adsorbed at the carbon tetrachloride/water interface in presence of a cationic surfactant (amine-functionalized polystyrene) in the oil phase. The inset shows the height profile along the red line. Reproduced with permission from [109]. Copyright 2019 American Chemical Society.

Methylated CNCs formed a dense monolayer with significantly higher surface coverage than unmodified CNCs [52] (Fig. 7C). It was argued above based on differences in surface pressure (10 mN/m for unmodified vs. 30 mN/m for methylated CNCs) that a higher surface coverage is likely for modified CNCs. Methylation further yielded thermosensitive CNCs which gelled and formed thick multilayers at 37°C [52]. The height bars in Fig. 7C correspond to ± 3 nm and 20 nm at 22°C and 37°C, respectively. CNCs esterified with C_{16} alkyl chains formed weakly aggregated clusters (Fig. 7D), which was attributed to attractive capillary forces [65], in contrast to unmodified CNCs which remain evenly dispersed due to electrostatic repulsion (Fig. 7A). Note that a comparably low concentration of esterified CNCs was used resulting in a low surface coverage, but a dense monolayer was achieved upon compression of the respective layer.

Niinivaara et al. [125] systematically probed the structure of differently modified NC-esters, namely cellulose acetate, cellulose acetate propionate, and cellulose triacetate, over a wide range of surface pressures. The study also considered layer displacement onto hydrophilic and hydrophobic substrates, revealing astonishing differences depending on which ester was used for modification, onto which substrates layers were transferred, and even at which surface pressure the layers were displaced. In general, smooth monolayers were observed on hydrophilic mica or silica, in agreement with the other cases discussed before (Figs. 7A-D). However, when transferred onto hydrophobic substrates, namely methylated silica or highly ordered pyrolytic graphite (HOPG), the NCs formed aggregated beads or strings with a characteristic striated structure, as shown exemplarily for cellulose triacetate transferred onto HOPG in Fig. 7E. At higher surface pressures the strings were compressed, resulting in closer string distances and increased alignment, as shown in the right part of Fig. 7E. For some cases the film displacement was not possible at all. For example, cellulose acetate butyrate could not be transferred onto silica, and cellulose acetate propionate films ruptured at high surface pressures, particularly for hydrophobic substrates. The study of Niinivaara et al. [125] demonstrates the complexity of interfacial film displacements and the many factors that may influence the results, as underlined by other studies that addressed NC-substrate interactions [126,127].

Interfacial displacement techniques are generally limited to the A/W interface. An alternative is in-situ liquid AFM directly at the O/W interface, as recently employed by Wu et al. [109]. The adsorption of CNCs at the carbon tetrachloride/water interface was investigated as the method requires an oil that is denser than water. Amine-functionalized polystyrene was dissolved in the carbon tetrachloride as cationic surfactant to promote CNC adsorption. A densely adsorbed layer of CNCs was observed, as shown in Fig. 7F. The surface coverage was significantly higher than for unmodified CNCs (Fig. 7A), in agreement with surfactant-induced CNF adsorption at the A/W interface (Fig. 7B). The AFM height profile (see inset) was used to estimate the CNC center-to-center distance, which was found to be 12.4 nm at pH 3. The positive charge of the surfactant was pH-dependent, resulting in a lower surface coverage and higher particle distance of 17.9 nm at pH 5. Hence, the charge of the employed surfactant effects the NC surface coverage, complementing the above discussion on the effect of surfactant charge on NC adsorption.

A possible technique that allows the imaging of O/W interfacial layers which has not been employed for NCs comprises the positioning of the substrate on a movable platform that is immersed in the aqueous phase [128,129]. The surface-active substance may then be spread at the interface and covered with a volatile oil. The immersed substrate is lifted through the O/W interface followed by evaporation of the oil and imaging of the adsorbed layer.

3.2.2. Structure analysis by interfacial reflectivity methods

Interfacial reflectivity methods are based on the change in dielectric properties or diffraction of photons or neutrons from interfacial thin films, allowing a noninvasive structure analysis. Habibi et al. [19] employed Brewster angle microscopy and ellipsometry to investigate NC layers adsorbed with the surfactant DODA, revealing a mixed and dense monolayer. The DODA content in the layers was determined to 25% by X-ray photoelectron spectroscopy. Upon compression of the layers, their thickness increased inversely proportional to the interface area, denoting that NCs were irreversibly adsorbed.

In the past few years, we employed neutron reflectometry to investigate the structure of unmodified CNCs and CNFs [16,17], methylated CNCs [51–53], and CNCs esterified with C_{16} alkyl groups [65]. The obtained reflection intensity as a function of the scattering vector can be fitted to extract morphological information on the thickness, roughness, and positioning of adsorbed layers [130]. For unmodified CNCs and CNFs, the measured interfacial layer was thinner than a single particle ($\approx$ 10 Å), suggesting that a loose monolayer was formed. Correlating the layer thickness to the particle height allowed an approximation of the surface coverage, which was 40% for CNFs and 20% for CNCs. The latter is in agreement with the coverage observed on displaced Langmuir-Schaefer films (Fig. 7A). These coverage values are lower compared to emulsions where around 60–80% were reported, as discussed above [123]. This discrepancy probably derives from the high energy input during emulsification, which facilitates to overcome the kinetic adsorption barrier. Further, differences within A/W and O/W interfaces may occur as addressed below. Besides the layer thickness, it was found that both CNCs and CNFs orient in the interfacial xy-plane, as is energetically favorable for anisotropic particles [131]. The scattering length density profiles in z-direction revealed that CNCs and CNFs were located primarily in the aqueous phase, allowing the qualitative conclusion that the contact angle θ of unmodified NCs is below 90°. The same layer morphology was observed after compression of adsorbed CNC layers, suggesting that the CNCs desorbed [16]. Adsorbed CNCs may be destabilized by their surface charge, the contact angle below 90°, or line tension induced by their anisotropy [39,132,133]. Nevertheless, CNC desorption from the A/W interface was not expected considering their irreversible adsorption and high stability generally observed in emulsions.

In contrast to unmodified NCs, Scheuble et al. reported a dense 30 Å monolayer with a diffusive secondary layer for methylated CNCs [52,53], probably due to lower electrostatic repulsion and increased hydrophobic interactions. The methylated CNCs were thermoresponsive and gelled into a thick 150 Å multilayer upon heating to 37°C, as previously shown for displaced layers of methylated CNCs in Fig. 7C. In another study, Scheuble et al. [51] investigated the structure of β-lactoglobulin-CNC multilayers, showing a primary protein monolayer followed by electrostatically complexed CNCs.

As indicated above, the contact angle θ of adsorbed particles may be assessed qualitatively from the scattering length density profile in z-direction [134]. Van den Berg et al. [65] developed a model that allows the quantitative determination of θ from reflectivity data by varying the CNC surface load and subphase contrast. It was used to study the positioning of CNCs with different degrees of esterification with C_{16} alkyl groups. The contact angle increased at higher degree of substitution (DS) and was 126°, 141°, and 156° for 0.1, 0.6, and 1.1 DS. The increasing contact angle demonstrates the effect of an increasing DS on NC hydrophobicity and particle positioning. It was already discussed above that NCs modified with short alkyl or carboxyl groups still form O/W emulsions [59,73,85], whereas NCs modified with longer hydrophobic moieties are preferentially wetted by the oil phase and form inverse W/O emulsions [9,63,68,86]. In contrast to the unmodified CNCs, the esterified CNCs did not desorb upon compression and the layers increased in thickness inversely proportional to the surface area, in agreement with CNCs adsorbed in presence of a surfactant [19]. Hence, NCs hydrophobized by surface-modifications or surfactant adsorption are more stably adsorbed compared to unmodified NCs, in agreement with the adsorption energies reported for unmodified (-5×10^3 k_BT [16–18]) and modified (-5×10^4 k_BT [58,59]) NCs obtained from

adsorption experiments using Eq. 1. The discussion on NC contact angle and stability is continued in a later section.

3.2.3. Interfacial rheology of adsorbed nanocellulose layers

Interfacial (2D) rheology has emerged as a key method to determine the mechanical properties of adsorbed interfacial layers. Two main forms of deformation are distinguished, namely interfacial shear rheology wherein layers are subjected to oscillatory shear at constant area, and interfacial dilatational rheology where layers are subjected to area compression-expansion cycles [135]. The interfacial rheology of unmodified CNCs at the A/W interface was addressed by Bertsch and Fischer [136]. We found that CNC layers do not reveal a significant dilatational viscoelasticity, which was attributed to their comparably low surface coverage of ≈ 20%. However, beyond a critical salt concentration of 10 mM NaCl the layers became increasingly elastic, as shown in Fig. 8A. This suggests that CNC attractive interactions are the origin of layer elasticity. The critical salt concentration is in good agreement with those known to allow for CNC interactions in bulk [137] and promote CNC adsorption at the interface [16,18], as previously shown in Figs. 3 B and E. In contrast to CNCs, CNFs formed viscoelastic layers also in absence of salt and independently of CNF charge density, potentially due to the increased aspect ratio and a higher surface coverage [17]. Although, Xu et al. [60] found that the viscoelasticity of acetylated CNF layers can still be enhanced by salt addition. The salt-induced viscoelasticity in CNC layers was associated with nonlinear strain-hardening in compression [136], as revealed by Lissajous-plots [138], whereas no significant nonlinearity was observed for CNFs [17].

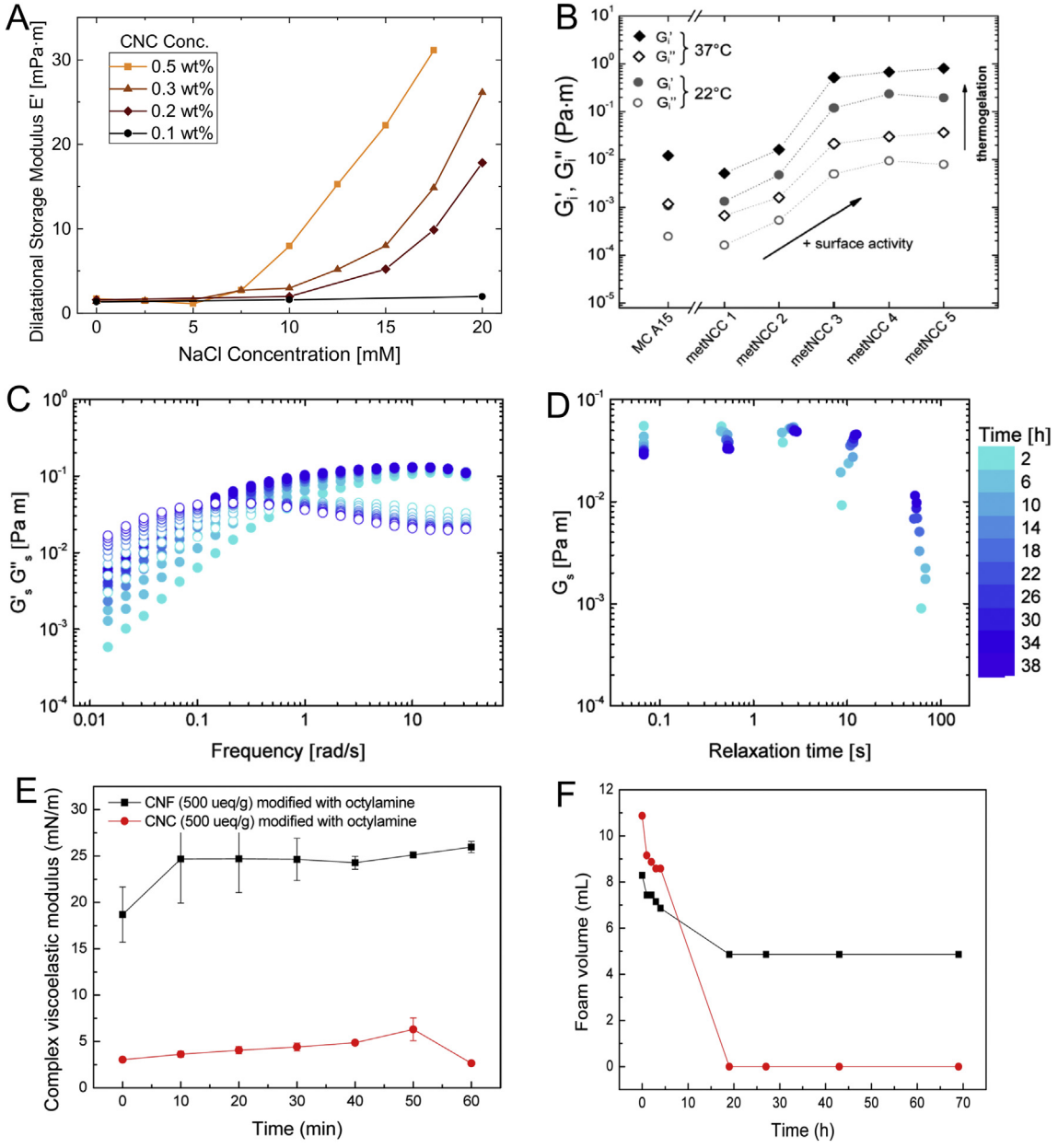

Fig. 8. (A) Interfacial dilatational storage modulus E' as a function of NaCl concentration at varying surface coverage (~ bulk concentration) of unmodified CNCs at the A/W interface. Reprinted with permission from [136]. Copyright 2019 American Chemical Society. (B) Interfacial shear storage G' and loss modulus G" for commercial methyl cellulose (MC A15) and methylated CNCs with increasing DS from left to right at 22°C and after thermogelation at 37°C. Reprinted with permission from [52]. Copyright 2016 American Chemical Society. (C) Dynamic frequency sweeps of C_{16}-alkylated CNCs (0.6 DS) determined at different time points as elaborated by the colour code and (D) respective relaxation time spectra. Reproduced from [66] with permission from AIP Publishing. (E) Complex dilatational modulus for CNFs and CNCs adsorbed at the A/W interface in combination with the cationic surfactant octylamine and (F) the stability of respective foams expressed as foam volume as a function of time. Reprinted with permission from [98]. Copyright 2015 American Chemical Society.

Scheuble et al. [52,53] reported an increasing interfacial shear elasticity for CNCs with increasing degree of methylation, as shown in Fig. 8B. This was attributed to higher CNC hydrophobic interactions, underlining the importance of attractive interactions in agreement with the findings for unmodified CNCs upon charge screening. CNC layers with higher shear moduli were also more brittle, i.e. showed nonlinear behavior at a lower critical strain. The methylated CNCs thermogelled at 37°C, resulting in a tenfold increase in interfacial viscoelasticity [52,53]. It was previously shown in Fig. 7C and discussed in the neutron reflectivity section that methylated CNCs thermogel from a diffusive 30 Å layer to a thick 150 Å multilayer. Scheuble et al. [51–53] also introduced the use of interfacial rheology with simultaneous subphase exchange to probe the in vitro digestion of adsorbed interfacial layers, demonstrating that the thermogelled methylated CNC layers resist simulated gastric conditions.

As discussed above, esterified CNCs form weakly aggregated clusters at the A/W interface (Fig. 7C) with a contact angle that increasingly exceeds 90° at higher DS [65,66]. The structure of separated CNC clusters resulted in a Maxwellian frequency behavior and allowed the calculation of characteristic relaxation time spectra as shown in Figs. 8C and D, which is rarely observed for 2D interfacial layers. Three to five relaxation times were found for the esterified CNC layers, which was attributed to the formation of clusters with varying size. A shift towards longer relaxation times was observed upon layer aging, potentially due to an increase in cluster size. More viscoelastic layers were found at higher DS and thus, hydrophobicity. This effect of NC hydrophobicity on viscoelasticity is interesting considering that θ increasingly deviates from 90°, where the highest viscoelasticity is generally observed [139]. These findings for unmodified, methylated, and esterified CNCs underline that attractive interactions are crucial for the viscoelasticity of interfacial particle layers.

Cervin et al. [22,98] investigated the interfacial rheology of surfactant-enhanced CNC and CNF layers (Fig. 8E) and its effect on foam stability (Fig. 8F). CNFs formed significantly more elastic layers than CNCs and elasticity was enhanced by salt addition, in good agreement with findings from unmodified CNCs and CNFs [17,60,136]. Consequently, CNFs were able to form more stable foams compared to CNCs. Besides higher interfacial viscoelasticity, the enhanced foam stability was attributed to the ability of CNFs to extend into the bulk, resulting in additional bulk stabilization and decreased drainage. These results were confirmed by Xiang et al. [113], who reported increased foam stability of surfactant-CNF mixtures compared to pure surfactants, which was attributed to an increase in both interfacial and bulk elasticity.

3.3. Nanocellulose contact angle at various subphases

It appears that the contact angle θ, i.e. the positioning of NCs in the three-phase contact line, is one of the main remaining questions regarding the structural aspects of NC layers. Contact angle measurements of particles in the nanorange remain challenging. Traditional immobilization and imaging techniques allow contact angle determinations for particles as small as 100 nm [43]. Recent developments such as freeze-fracture shadow-casting cryo-SEM [140] or multiple angle of incidence ellipsometry [141] have pushed the boundary to as low as 10 nm diameter. As NCs generally orient in the interfacial boundary and are < 10 nm thick, they are still below the resolution limit. Clint et al. [142] presented a straightforward approach that derives θ from pressure-area isotherms, which however requires the 2D close-packing density, which can hardly be approximated satisfactorily for anisotropic and polydisperse NCs.

As already addressed above, SANS with additional contrast variation [121] and neutron reflectometry [16,17] were used to assess θ of unmodified NCs in O/W emulsions and planar A/W interfaces, respectively. Both techniques provided consistent qualitative information that the NCs are primarily wetted by the aqueous phase, and thus $\theta < 90°$. Van den Berg et al. [65] employed neutron reflectometry with additional contrast variation to determine θ quantitatively for CNCs with different DS, as elaborated above. However, the high number of parameters in the model requires to vary the surface coverage along with the subphase contrast. As layers of unmodified NCs are close to the spatial resolution of the employed reflectivity setup, we could not apply the model in our later reflectometry studies on unmodified CNCs and CNFs [16,17].

An alternative method comprises the formation of a solid NC surface which is covered with an aqueous solution, allowing the determination of the three phase air-solid-liquid contact angle. Li et al. [49] found $\theta =$ 27 and 44° for a primarily hydrophilic and a more hydrophobic CNC crystal allomorph, respectively. Jin et al. [56] reported $\theta = 70–80°$ for ethylated NCs. Hu et al. [99] employed this method to assess θ for CNCs with increasing surfactant coverage, as shown in Fig. 5C. An increasing θ was observed for higher surfactant coverage with an inversion at the CMC of the surfactants, indicating the formation of surfactant multilayers. These studies underline that unmodified NCs adsorb at low θ and it is increased at higher NC surface hydrophobicity. This method seems to be a straightforward approach to get insights on θ and even provides quantitative results. However, it is not entirely clear to what extent the results can be translated to NC adsorption at fluid interfaces with freely movable and interacting particles. For instance, the effective θ of anisotropic particles diverges from 90° compared to theoretical values predicted by Young-Laplace's equation due to line tension contributions, which are enhanced at increasing aspect ratio [132,133].

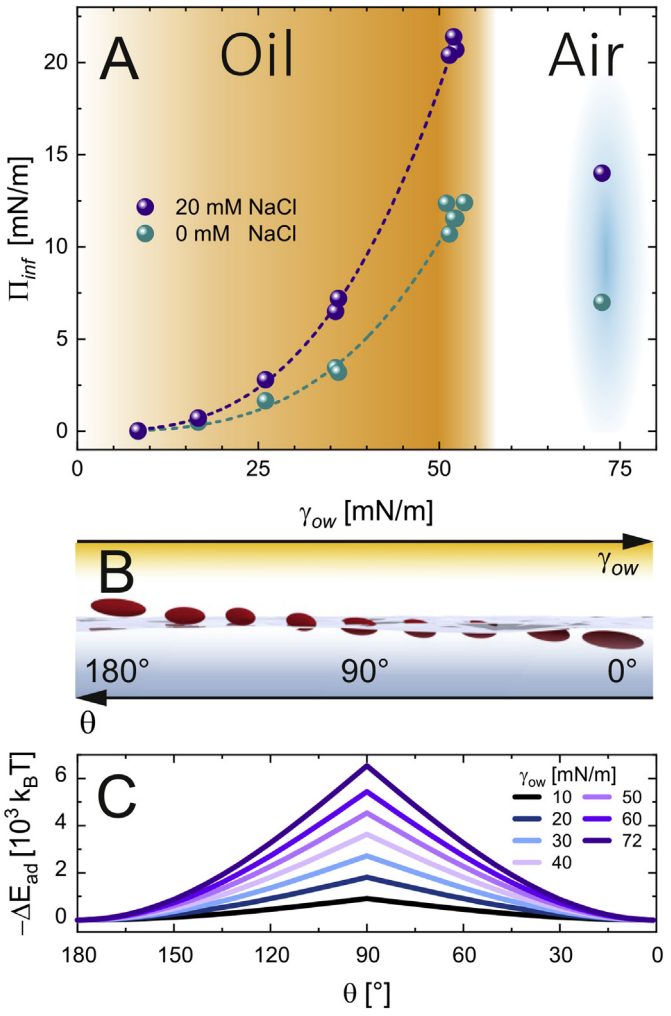

Fig. 9. (A) Equilibrium surface pressure Π_{inf} as a function of interface tension for CNCs adsorbed at the air and oil interfaces with varying interface tension γ_{ow}. (B) Scheme of particle immersion and (C) related particle adsorption energy ΔE at subphases with varying γ_{ow}. Reproduced with permission from [18] - published by The Royal Society of Chemistry.

Another approach to assess θ of unmodified CNCs at various interfaces was presented by Bergfreund et al. [18]. CNCs were adsorbed at air and different oils with a wide range of polarity, and thus varying interface tension γ_{ow}. The equilibrium surface pressure Π_{inf} of CNCs adsorbed at different oils followed a power law as a function of γ_{ow}, as shown in Fig. 9A. As elaborated in Eqs. 1 and 2, the measured Π derives from the the adsorption energy of a single particle ΔE, which again derives from γ_{ow} and θ, as visualized in Figs. 9B and C. The fact that lower Π_{inf} are attained for the A/W interface ($\gamma_{aw} = 72.4$ mN/m) compared to n-alkanes ($\gamma_{ow} = 51$ mN/m) allowed the conclusion that θ is shifted closer to 90° at O/W interfaces compared to the A/W interface. It is consequential that θ further approaches 90° for more polar oils, although Π_{inf} decreases due to the lower γ_{ow}. Hence, the θ of NCs is shifted towards 90° for more polar oils, however, their adsorption energy becomes negligible, as confirmed by the impeded emulsification with polar oils [14,18]. Eq. 1 also includes the surface coverage, which has not been assessed and may vary within the different oils, particularly as oil properties increase in importance upon further particle immersion [143].

To conclude, unmodified NCs adsorb at $\theta < 90°$ at fluid interfaces, and θ is shifted towards 90° at oils with increasing polarity. This suggest an energetically unfavorable contact angle of NCs at the A/W interface, which may explain why unmodified CNCs desorbed upon area compression [16]. It was recently argued that this could be the reason why unmodified NCs are not able to stabilize foams without further surface modification, whereas no such problems occur for O/W emulsions [17,18]. In order to form stable foams or push θ beyond 90°, the hydrophobicity of NCs needs to be increased by covalent surface modifications or surfactants that adsorb at the NC surface, as elaborated in previous sections. Nevertheless, θ of unmodified NCs at fluid interfaces remains to be elucidated quantitatively.

4. Concluding remarks

Established less than 10 years ago, the interfacial stabilization by NCs has attracted attention from various fields owed to the outstanding stability and biocompatible nature of NC stabilized colloids. While the formation and characterization of NC stabilized emulsions are well established, the fundamental aspects of NC adsorption and structure at fluid interfaces were addressed more recently as emphasized in this review. The new insights on NC adsorption at fluid interfaces have already helped to answer some fundamental questions in the field, the most striking probably being the reduction in surface tension which has caused many speculations in the past as outlined by a previous review [10]. Another mystery of unmodified NCs has always been their inability to form stable foams while forming very stable emulsions. Recent findings suggest an unfavorable contact angle and reversible adsorption of NCs at A/W interfaces as potential reasons [16–18]. At the same time, the quantitative determination of NC contact angles at fluid interfaces remains one of the major challenges in the field.

Another intriguing finding is the importance of the chosen oil, which alters the adsorption behavior of NCs [18] as well as the droplet size and stability of formed emulsions [14], and may significantly impede the comparability of results obtained with different oils. Hence, it is important to not only report aqueous phase parameters like pH and ionic strength, but also oil properties like interface tension, viscosity, and purity to guarantee comparability within scientific results. It has further come to our attention that many studies report either on the interfacial behavior of NCs or the properties of NC-stabilized foams and emulsions, whereas far less studies cover both aspects of NC interfacial stabilization. As a consequence, there seems to be a gap between fundamental interface studies and more applied studies. For instance, the structure and coverage reported in emulsions diverges from findings at 2D interfaces, making it difficult to conclude on the surface tension reduction in emulsions. We would like to encourage the community to combine these aspects more frequently in the future to close this gap.

To conclude, many fundamental question regarding NC interfacial stabilization could be resolved in the first decade of this comparably young field, with certain challenges still to be addressed. We expect that the new insights on NC adsorption and their interfacial layers will facilitate bottom-up approaches, i.e. the design of NC interfacial layers with desired properties which are then translated to macroscopic materials. NC stabilized colloids are already being established in various cutting-edge applications, including novel bio-nanocomposites [51,53,106,120,144], gastric stable delivery systems [13,15,68,117,145,146], or the formulation of low solid 3D printing inks [147,148], which could benefit from these possibilities.

Notes

The authors declare no conflict of interest.

Acknowledgments

This work was supported by the Swiss National Science Foundation, Project No. 200021- 175994.

References

[1] Turbak AF, Snyder FW, Sandberg KR. Microfibrillated cellulose, a new cellulose product: properties, uses, and commercial potential. J Appl Polym Sci: Appl Polym Symp 1983;37:815–27.
[2] Isogai A, Saito T, Fukuzumi H. TEMPO-oxidized cellulose nanofibers. Nanoscale 2011;3(1):71–85. https://doi.org/10.1039/c0nr00583e.
[3] Habibi Y. Key advances in the chemical modification of nanocelluloses. Chem Soc Rev 2014;43(43):1519–42. https://doi.org/10.1039/c3cs60204d.
[4] Jorfi M, Foster EJ. Recent advances in nanocellulose for biomedical applications. J Appl Polym Sci 2015;132(14):41719. https://doi.org/10.1002/app.41719.
[5] Saito T, Kuramae R, Wohlert J, Berglund LA, Isogai A. An ultrastrong nanofibrillar biomaterial: the strength of single cellulose nanofibrils revealed via sonication-induced fragmentation. Biomacromolecules 2013;14(1):248–53. https://doi.org/10.1021/bm301674e.
[6] Revol J-F, Bradford H, Giasson J, Marchessault R, Gray D. Helicoidal self-ordering of cellulose microfibrils in aqueous suspension. Int J Biol Macromol 1992;14(3):170–2. https://doi.org/10.1016/S0141-8130(05)80008-X.
[7] De France KJ, Hoare T, Cranston ED. Review of hydrogels and aerogels containing nanocellulose. Chem Mater 2017;29(11):4609–31. https://doi.org/10.1021/acs.chemmater.7b00531.
[8] Kalashnikova I, Bizot H, Cathala B, Capron I. New Pickering emulsions stabilized by bacterial cellulose nanocrystals. Langmuir 2011;27(12):7471–9. https://doi.org/10.1021/la200971f.
[9] Xhanari K, Syverud K, Stenius P. Emulsions stabilized by microfibrillated cellulose: the effect of hydrophobization, concentration and O/W ratio. J Dispers Sci Technol 2011;32(3):447–52. https://doi.org/10.1080/01932691003658942.
[10] Capron I, Rojas OJ, Bordes R. Behavior of nanocelluloses at interfaces. Curr Opin Colloid Interface Sci 2017;29:83–95. https://doi.org/10.1016/j.cocis.2017.04.001.
[11] Fujisawa S, Togawa E, Kuroda K. Nanocellulose-stabilized Pickering emulsions and their applications. Sci Technol Adv Mater 2017;18(1):959–71. https://doi.org/10.1080/14686996.2017.1401423.
[12] Capron I, Cathala B. Surfactant-free high internal phase emulsions stabilized by cellulose nanocrystals. Biomacromolecules 2013;14(2):291–6. https://doi.org/10.1021/bm301871k.
[13] Scheuble N, Schaffner J, Schumacher M, Windhab EJ, Liu D, Parker H, et al. Tailoring emulsions for controlled lipid release: establishing in vitro-in vivo correlation for digestion of lipids. ACS Appl Mater Interfaces 2018;10(21):17571–81. https://doi.org/10.1021/acsami.8b02637.
[14] Bai L, Lv S, Xiang W, Huan S, McClements DJ, Rojas OJ. Oil-in-water Pickering emulsions via microuidization with cellulose nanocrystals: 1. Formation and stability. Food Hydrocoll 2019;96(April):699–708. https://doi.org/10.1016/j.foodhyd.2019.04.038.
[15] Bai L, Lv S, Xiang W, Huan S, McClements DJ, Rojas OJ. Oil-in-water Pickering emulsions via microuidization with cellulose nanocrystals: 2. In vitro lipid digestion. Food Hydrocoll 2019;96(April):709–16. https://doi.org/10.1016/j.foodhyd.2019.04.039.
[16] Bertsch P, Diener M, Adamcik J, Scheuble N, Geue T, Mezzenga R, et al. Adsorption and interfacial layer structure of unmodified nanocrystalline cellulose at air/water interfaces. Langmuir 2018;34(50):15195–202. https://doi.org/10.1021/acs.langmuir.8b03056.
[17] Bertsch P, Arcari M, Geue T, Mezzenga R, Nyström G, Fischer P. Designing cellulose nanofibrils for stabilization of fluid interfaces. Biomacromolecules 2019;20(12):4574–80. https://doi.org/10.1021/acs.biomac.9b01384.
[18] Bergfreund J, Sun Q, Fischer P, Bertsch P. Adsorption of charged anisotropic nanoparticles at oil-water interfaces. Nanoscale Adv 2019;1(11):4308–12. https://doi.org/10.1039/C9NA00506D.

[19] Habibi Y, Foulon L, Aguié-Béghin V, Molinari M, Douillard R. Langmuir-Blodgett films of cellulose nanocrystals: preparation and characterization. J Colloid Interface Sci 2007;316(2):388–97. https://doi.org/10.1016/j.jcis.2007.08.041.

[20] Campbell AL, Holt BL, Stoyanov SD, Paunov VN. Scalable fabrication of anisotropic micro-rods from food-grade materials using an in shear ow dispersion-solvent attrition technique. J Mater Chem 2008;18(34):4074–8. https://doi.org/10.1039/b807738j.

[21] Dhar N, Au D, Berry RC, Tam KC. Interactions of nanocrystalline cellulose with an oppositely charged surfactant in aqueous medium. Colloids Surf A Physicochem Eng Asp 2012;415:310–9. https://doi.org/10.1016/j.colsurfa.2012.09.010.

[22] Cervin NT, Andersson L, Ng JBS, Olin P, Bergström L, Wågberg L. Lightweight and strong cellulose materials made from aqueous foams stabilized by nanofibrillated cellulose. Biomacromolecules 2013;14(2):503–11. https://doi.org/10.1021/bm301755u.

[23] Saito T, Kimura S, Nishiyama Y, Isogai A. Cellulose nanofibers prepared by TEMPOmediated oxidation of native cellulose. Biomacromolecules 2007;8(8):2485–91. https://doi.org/10.1021/bm0703970.

[24] Nyström G, Arcari M, Adamcik J, Usov I, Mezzenga R. Nanocellulose fragmentation mechanisms and inversion of chirality from the single particle to the cholesteric phase. ACS Nano 2018;12(6):5141–8. https://doi.org/10.1021/acsnano.8b00512.

[25] Li Q, Renneckar S. Supramolecular structure characterization of molecularly thin cellulose I nanoparticles. Biomacromolecules 2011;12(3):650–9. https://doi.org/10.1021/bm101315y.

[26] Arcari M, Zuccarella E, Axelrod R, Adamcik J, Sánchez-Ferrer A, Mezzenga R, et al. Nanostructural properties and twist periodicity of cellulose nanofibrils with variable charge density. Biomacromolecules 2019;20(3):1288–96. https://doi.org/10.1021/acs.biomac.8b01706.

[27] Yamane C, Aoyagi T, Ago M, Sato K, Okajima K, Takahashi T. Two different surface properties of regenerated cellulose due to structural anisotropy. Polym J 2006;38(8):819–26. https://doi.org/10.1295/polymj.PJ2005187.

[28] Mazeau K. On the external morphology of native cellulose microfibrils. Carbohydr Polym 2011;84(1):524–32. https://doi.org/10.1016/j.carbpol.2010.12.016.

[29] Kutuzov S, He J, Tangirala R, Emrick T, Russell TP, Böker A. On the kinetics of nanoparticle self-assembly at liquid/liquid interfaces. Phys Chem Chem Phys 2007;9(48):6351–8. https://doi.org/10.1039/b710060b.

[30] Hua X, Frechette J, Bevan MA. Nanoparticle adsorption dynamics at uid interfaces. Soft Matter 2018;14(19):3818–28. https://doi.org/10.1039/C8SM00273H.

[31] Du K, Glogowski E, Emrick T, Russell TP, Dinsmore AD. Adsorption energy of nanoand microparticles at liquidliquid interfaces. Langmuir 2010;26(15):12518–22. https://doi.org/10.1021/la100497h.

[32] Binks BP, Horozov TS. Colloidal particles at liquid interfaces. Cambridge University Press; 2006.

[33] Leunissen ME, Zwanikken J, van Roij R, Chaikin PM, van Blaaderen A. Ion partitioning at the oil-water interface as a source of tunable electrostatic effects in emulsions with colloids. Phys Chem Chem Phys 2007;9(48):6405–14. https://doi.org/10.1039/b705094a.

[34] Wang H, Singh V, Behrens SH. Image charge effects on the formation of Pickering emulsions. J Phys Chem Lett 2012;3(20):2986–90. https://doi.org/10.1021/jz300909z.

[35] Dugyala VR, Anjali TG, Upendar S, Mani E, Basavaraj MG. Nano ellipsoids at the uid-uid interface: effect of surface charge on adsorption, buckling and emulsification. Faraday Discuss 2016;186:419–34. https://doi.org/10.1039/C5FD00136F.

[36] Dugyala VR, Muthukuru JS, Mani E, Basavaraj MG. Role of electrostatic interactions in the adsorption kinetics of nanoparticles at uiduid interfaces. Phys Chem Chem Phys 2016;18(7):5499–508. https://doi.org/10.1039/C5CP05959C.

[37] Reincke F, Hickey SG, Kegel WK, Vanmaekelbergh D. Spontaneous assembly of a monolayer of charged gold nanocrystals at the water/oil interface. Angew Chem Int Ed 2004;43(4):458–62. https://doi.org/10.1002/anie.200352339.

[38] Pandey A, Derakhshandeh M, Kedzior SA, Pilapil B, Shomrat N, Segal-Peretz T, et al. Role of interparticle interactions on microstructural and rheological properties of cellulose nanocrystal stabilized emulsions. J Colloid Interface Sci 2018;532:808–18. https://doi.org/10.1016/j.jcis.2018.08.044.

[39] Foret L, Würger A. Electric-field induced capillary interaction of charged particles at a polar interface. Phys Rev Lett 2003;92(5). https://doi.org/10.1103/PhysRevLett.92.058302 058302.

[40] Kalashnikova I, Bizot H, Cathala B, Capron I. Modulation of cellulose nanocrystals amphiphilic properties to stabilize oil/water interface. Biomacromolecules 2012;13(1):267–75. https://doi.org/10.1021/bm201599j.

[41] Smith KB, Tisserant J-N, Assenza S, Arcari M, Nyström G, Mezzenga R. Confinement-induced ordering and self-folding of cellulose nanofibrils. Adv Sci 2019;6(4):1801540. https://doi.org/10.1002/advs.201801540.

[42] Botto L, Lewandowski EP, Cavallaro M, Stebe KJ. Capillary interactions between anisotropic particles. Soft Matter 2012;8(39):9957–71. https://doi.org/10.1039/c2sm25929j.

[43] Zanini M, Isa L. Particle contact angles at uid interfaces: pushing the boundary beyond hard uniform spherical colloids. J Phys Condens Matter 2016;28(31):313002. https://doi.org/10.1088/0953-8984/28/31/313002.

[44] Jiang F, Hsieh Y-L. Holocellulose nanocrystals: Amphiphilicity, oil/water emulsion, and self-assembly. Biomacromolecules 2015;16(4):1433–41. https://doi.org/10.1021/acs.biomac.5b00240.

[45] Rojas OJ, Bullón J, Ysambertt F, Forgiarini A, Salager J-L, Argyropoulos DS. Lignins as emulsion stabilizers. Mater. Chem. Energy from for. Biomass, American Chemical Society; 2007. p. 182–99. https://doi.org/10.1021/bk-2007-0954.ch012.

[46] Hubbe MA, Rojas OJ, Lucia LA. Green modification of surface characteristics of cellulosic materials at the molecular or nano scale: a review. BioResources 2015;10(3):6095–206. https://doi.org/10.15376/biores.10.3.Hubbe.

[47] Peddireddy KR, Nicolai T, Benyahia L, Capron I. Stabilization of water-in-water emulsions by nanorods. ACS Macro Lett 2016;5(3):283–6. https://doi.org/10.1021/acsmacrolett.5b00953.

[48] Ben Ayed E, Cochereau R, Dechancé C, Capron I, Nicolai T, Benyahia L. Water-inwater emulsion gels stabilized by cellulose nanocrystals. Langmuir 2018;34(23):6887–93. https://doi.org/10.1021/acs.langmuir.8b01239.

[49] Li X, Li J, Gong J, Kuang Y, Mo L, Song T. Cellulose nanocrystals (CNCs) with different crystalline allomorph for oil in water Pickering emulsions. Carbohydr Polym 2018;183(November 2017):303–10. https://doi.org/10.1016/j.carbpol.2017.12.085.

[50] Eyley SS, Thielemans W. Surface modification of cellulose nanocrystals. Nanoscale 2014;6(14):7764–79. https://doi.org/10.1039/c4nr01756k.

[51] Scheuble N, Geue T, Windhab EJ, Fischer P. Tailored interfacial rheology for gastric stable adsorption layers. Biomacromolecules 2014;15(8):3139–45. https://doi.org/10.1021/bm500767c.

[52] Scheuble N, Geue T, Kuster S, Adamcik J, Mezzenga R, Windhab EJ, et al. Mechanically enhanced liquid interfaces at human body temperature using thermosensitive methylated nanocrystalline cellulose. Langmuir 2016;32(5):1396–404. https://doi.org/10.1021/acs.langmuir.5b04231.

[53] Scheuble N, Lussi M, Geue T, Carrière F, Fischer P. Blocking gastric lipase adsorption and displacement processes with viscoelastic biopolymer adsorption layers. Biomacromolecules 2016;17(10):3328–37. https://doi.org/10.1021/acs.biomac.6b01081.

[54] Zhang Y, Shitta A, Meredith JC, Behrens SH. Bubble meets droplet: particle-assisted reconfiguration of wetting morphologies in colloidal multiphase systems. Small 2016;12(24):3309–19. https://doi.org/10.1002/smll.201600799.

[55] Campbell AL, Stoyanov SD, Paunov VN. Fabrication of functional anisotropic foodgrade micro-rods with micro-particle inclusions with potential application for enhanced stability of food foams. Soft Matter 2009;5(5):1019–23. https://doi.org/10.1039/b812706a.

[56] Jin H, Zhou W, Cao J, Stoyanov SD, Blijdenstein TB, De Groot PW, et al. Super stable foams stabilized by colloidal ethyl cellulose particles. Soft Matter 2012;8(7):2194–205. https://doi.org/10.1039/c1sm06518a.

[57] Bizmark N, Ioannidis MA, Henneke DE. Irreversible adsorption-driven assembly of nanoparticles at uid interfaces revealed by a dynamic surface tension probe. Langmuir 2014;30(3):710–7. https://doi.org/10.1021/la404357j.

[58] Bizmark N, Ioannidis MA. Effects of ionic strength on the colloidal stability and interfacial assembly of hydrophobic ethyl cellulose nanoparticles. Langmuir 2015;31(34):9282–9. https://doi.org/10.1021/acs.langmuir.5b01857.

[59] Bizmark N, Ioannidis MA. Ethyl cellulose nanoparticles at the alkane-water interface and the making of Pickering emulsions. Langmuir 2017;33(40):10568–76. https://doi.org/10.1021/acs.langmuir.7b02051.

[60] Xu H-N, Li Y-H, Zhang L. Driving forces for accumulation of cellulose nanofibrils at the oil/water interface. Langmuir 2018;34(36):10757–63. https://doi.org/10.1021/acs.langmuir.8b02310.

[61] Xhanari K, Syverud K, Chinga-Carrasco G, Paso K, Stenius P. Structure of nanofibrillated vellulose layers at the O/W Interface. J Colloid Interface Sci 2011;356(1):58–62. https://doi.org/10.1016/j.jcis.2010.12.083.

[62] Zhang X, Shao Z, Zhou Y, Wei J, He W, Wang S, et al. Redispersibility of cellulose nanoparticles modified by phenyltrimethoxysilane and its application in stabilizing Pickering emulsions. J Mater Sci 2019;54(17):11713–25. https://doi.org/10.1007/s10853-019-03691-6.

[63] Cunha AG, Mougel JB, Cathala B, Berglund LA, Capron I. Preparation of double Pickering emulsions stabilized by chemically tailored nanocelluloses. Langmuir 2014;30(31):9327–35. https://doi.org/10.1021/la5017577.

[64] Saidane D, Perrin E, Cherhal F, Guellec F, Capron I. Some modification of cellulose nanocrystals for functional Pickering emulsions. Philos Trans R Soc A Math Phys Eng Sci 2016;374(2072):1–11.

[65] van den Berg MEH, Kuster S, Windhab EJ, Adamcik J, Mezzenga R, Geue T, et al. Modifying the contact angle of anisotropic cellulose nanocrystals: effect on interfacial rheology and structure. Langmuir 2018;34(37):10932–42. https://doi.org/10.1021/acs.langmuir.8b00623.

[66] van den Berg MEH, Kuster S, Windhab EJ, Sagis LMC, Fischer P. Nonlinear shear and dilatational rheology of viscoelastic interfacial layers of cellulose nanocrystals. Phys Fluids 2018;30(7):072103. https://doi.org/10.1063/1.5035334.

[67] Chen QH, Zheng J, Xu YT, Yin SW, Liu F, Tang CH. Surface modification improves fabrication of Pickering high internal phase emulsions stabilized by cellulose nanocrystals. Food Hydrocoll 2018;75:125–30. https://doi.org/10.1016/j.foodhyd.2017.09.005.

[68] Zhang Z, Tam KC, Wang X, Sèbe G. Inverse Pickering emulsions stabilized by cinnamate modified cellulose nanocrystals as templates to prepare silica colloidosomes. ACS Sustain Chem Eng 2018;6(2):2583–90. https://doi.org/10.1021/acssuschemeng.7b04061.

[69] Tang C, Chen Y, Luo J, Low MY, Shi Z, Tang J, et al. Pickering emulsions stabilized by hydrophobically modified nanocellulose containing various structural characteristics. Cellulose 2019;26(13–14):7753–67. https://doi.org/10.1007/s10570-019-02648-x.

[70] Azzam F, Heux L, Putaux JL, Jean B. Preparation by grafting onto, characterization, and properties of thermally responsive polymer-decorated cellulose nanocrystals. Biomacromolecules 2010;11(12):3652–9. https://doi.org/10.1021/bm101106c.

[71] Saigal T, Dong H, Matyjaszewski K, Tilton RD. Pickering emulsions stabilized by nanoparticles with thermally responsive grafted polymer brushes. Langmuir 2010;26(19):15200–9. https://doi.org/10.1021/la1027898.

[72] Zoppe JO, Venditti RA, Rojas OJ. Pickering emulsions stabilized by cellulose nanocrystals grafted with thermo-responsive polymer brushes. J Colloid Interface Sci 2012;369(1):202–9. https://doi.org/10.1016/j.jcis.2011.12.011.

[73] Sèbe G, Ham-Pichavant F, Pecastaings G. Dispersibility and emulsion-stabilizing effect of cellulose nanowhiskers esterified by vinyl acetate and vinyl cinnamate. Biomacromolecules 2013;14(8):2937–44. https://doi.org/10.1021/bm400854n.
[74] Tang J, Lee MFX, Zhang W, Zhao B, Berry RM, Tam KC. Dual responsive Pickering emulsion stabilized by poly[2-(dimethylamino) ethyl methacrylate] grafted cellulose nanocrystals. Biomacromolecules 2014;15(8):3052–60. https://doi.org/10.1021/bm500663w.
[75] Tang J, Berry RM, Tam KC. Stimuli-responsive cellulose nanocrystals for surfactantfree oil harvesting. Biomacromolecules 2016;17(5):1748–56. https://doi.org/10.1021/acs.biomac.6b00144.
[76] Tang C, Spinney S, Shi Z, Tang J, Peng B, Luo J, et al. Amphiphilic cellulose nanocrystals for enhanced Pickering emulsion stabilization. Langmuir 2018;34(43):12897–905. https://doi.org/10.1021/acs.langmuir.8b02437.
[77] Hiranphinyophat S, Asaumi Y, Fujii S, Iwasaki Y. Surface grafting polyphosphoesters on cellulose nanocrystals to improve the emulsification efficacy. Langmuir 2019;35(35):11443–51. https://doi.org/10.1021/acs.langmuir.9b01584.
[78] Glasing J, Jessop PG, Champagne P, Cunningham MF. Graft-modified cellulose nanocrystals as CO2-switchable Pickering emulsifiers. Polym Chem 2018;9(28):3864–72. https://doi.org/10.1039/c8py00417j.
[79] Li W, Ju B, Zhang S. Novel amphiphilic cellulose nanocrystals for pH-responsive Pickering emulsions. Carbohydr Polym 2020;229:115401. https://doi.org/10.1016/j.carbpol.2019.115401.
[80] Liu S, Zhu Y, Wu Y, Lue A, Zhang C. Hydrophobic modification of regenerated cellulose microparticles with enhanced emulsifying capacity for O/W Pickering emulsion. Cellulose 2019;26(10):6215–28. https://doi.org/10.1007/s10570-019-02538-2.
[81] Mackie AR, Gunning AP, Wilde PJ, Morris VJ. Orogenic displacement of protein from the air/water interface by competitive adsorption. J Colloid Interface Sci 1999;210(1):157–66. https://doi.org/10.1006/jcis.1998.5941.
[82] Rühs PA, Storz F, López Gómez YA, Haug M, Fischer P. 3D bacterial cellulose biofilms formed by foam templating. npj Biofilms Microbiomes 2018;4(1):21. https://doi.org/10.1038/s41522-018-0064-3.
[83] Zhang Y, Karimkhani V, Makowski BT, Samaranayake G, Rowan SJ. Nanoemulsions and nanolatexes stabilized by hydrophobically functionalized cellulose nanocrystals. Macromolecules 2017;50(16):6032–42. https://doi.org/10.1021/acs.macromol.7b00982.
[84] Jiménez Saelices C, Capron I. Design of Pickering micro- and nanoemulsions based on the structural characteristics of nanocelluloses. Biomacromolecules 2018;19(2):460–9. https://doi.org/10.1021/acs.biomac.7b01564.
[85] Gong X, Wang Y, Chen L. Enhanced emulsifying properties of wood-based cellulose nanocrystals as Pickering emulsion stabilizer. Carbohydr Polym 2017;169:295–303. https://doi.org/10.1016/j.carbpol.2017.04.024.
[86] Werner A, Schmitt V, Sèbe G, Héroguez V. Convenient synthesis of hybrid polymer materials by AGET-ATRP polymerization of Pickering emulsions stabilized by cellulose nanocrystals grafted with reactive moieties. Biomacromolecules 2019;20(1):490–501. https://doi.org/10.1021/acs.biomac.8b01482.
[87] Lee KY, Blaker JJ, Murakami R, Heng JY, Bismarck A. Phase behavior of medium and high internal phase water-in-oil emulsions stabilized solely by hydrophobized bacterial cellulose nanofibrils. Langmuir 2014;30(2):452–60. https://doi.org/10.1021/la4032514.
[88] Guo J, Du W, Gao Y, Cao Y, Yin Y. Cellulose nanocrystals as water-in-oil Pickering emulsifiers via intercalative modification, colloids surfaces A Physicochem. Eng Asp 2017;529(April):634–42. https://doi.org/10.1016/j.colsurfa.2017.06.056.
[89] Lee KY, Blaker JJ, Heng JY, Murakami R, Bismarck A. PH-triggered phase inversion and separation of hydrophobised bacterial cellulose stabilised Pickering emulsions. React Funct Polym 2014;85:208–13. https://doi.org/10.1016/j.reactfunctpolym.2014.09.016.
[90] Peng J, Liu Q, Xu Z, Masliyah J. Synthesis of interfacially active and magnetically responsive nanoparticles for multiphase separation applications. Adv Funct Mater 2012;22(8):1732–40. https://doi.org/10.1002/adfm.201102156.
[91] Wohlhauser S, Delepierre G, Labet M, Morandi G, Thielemans W, Weder C, et al. Grafting polymers from cellulose nanocrystals: synthesis, properties, and applications. Macromolecules 2018;51(16):6157–89. https://doi.org/10.1021/acs.macromol.8b00733.
[92] Aaen R, Brodin F, Simon S, Heggset E, Syverud K. Oil-in-water emulsions stabilized by cellulose nanofibrils-the effects of ionic strength and pH. Nanomaterials 2019;9(2):259. https://doi.org/10.3390/nano9020259.
[93] Mikulcová V, Bordes R, Minaík A, Kašpárková V. Pickering oil-in-water emulsions stabilized by carboxylated cellulose nanocrystals - effect of the pH. Food Hydrocoll 2018;80:60–7. https://doi.org/10.1016/j.foodhyd.2018.01.034.
[94] Low LE, Tey BT, Ong BH, Chan ES, Tang SY. Dispersion stability, magnetivity and wettability of cellulose nanocrystal (CNC)-dispersed superparamagnetic Fe3O4 nanoparticles: impact of CNC concentration. RSC Adv 2016;6(114):113132–8. https://doi.org/10.1039/c6ra16109j.
[95] Low LE, Tan LTH, Goh BH, Tey BT, Ong BH, Tang SY. Magnetic cellulose nanocrystal stabilized Pickering emulsions for enhanced bioactive release and human colon cancer therapy. Int J Biol Macromol 2019;127:76–84. https://doi.org/10.1016/j.ijbiomac.2019.01.037.
[96] Low LE, Tey BT, Ong BH, Chan ES, Tang SY. Palm olein-in-water Pickering emulsion stabilized by Fe3O4-cellulose nanocrystal nanocomposites and their responses to pH. Carbohydr Polym 2017;155:391–9. https://doi.org/10.1016/j.carbpol.2016.08.091.
[97] Low LE, Tey BT, Ong BH, Tang SY. Unravelling pH-responsive behaviour of Fe3O4@CNCs-stabilized Pickering emulsions under the inuence of magnetic field. Polymer 2018;141:93–101. https://doi.org/10.1016/j.polymer.2018.03.001.
[98] Cervin NT, Johansson E, Benjamins J-W, Wågberg L. Mechanisms behind the stabilizing action of cellulose nanofibrils in wet-stable cellulose foams. Biomacromolecules 2015;16(3):822–31. https://doi.org/10.1021/bm5017173.
[99] Hu Z, Ballinger S, Pelton R, Cranston ED. Surfactant-enhanced cellulose nanocrystal Pickering emulsions. J Colloid Interface Sci 2015;439:139–48. https://doi.org/10.1016/j.jcis.2014.10.034.
[100] Brinatti C, Huang J, Berry RM, Tam KC, Loh W. Structural and energetic studies on the interaction of cationic surfactants and cellulose nanocrystals. Langmuir 2016;32(3):689–98. https://doi.org/10.1021/acs.langmuir.5b03893.
[101] Bai L, Xiang W, Huan S, Rojas OJ. Formulation and stabilization of concentrated edible oil-in-water emulsions based on electrostatic complexes of a food-grade cationic surfactant (ethyl lauroyl arginate) and cellulose nanocrystals. Biomacromolecules 2018;19(5):1674–85. https://doi.org/10.1021/acs.biomac.8b00233.
[102] Kedzior SA, Marway HS, Cranston ED. Tailoring cellulose nanocrystal and surfactant behavior in miniemulsion polymerization. Macromolecules 2017;50(7):2645–55. https://doi.org/10.1021/acs.macromol.7b00516.
[103] Carrillo CA, Nypelö TE, Rojas OJ. Cellulose nanofibrils for one-step stabilization of multiple emulsions (W/O/W) based on soybean oil. J Colloid Interface Sci 2015;445:166–73. https://doi.org/10.1016/j.jcis.2014.12.028.
[104] Li Z, Bai B, Xu D, Meng Z, Ma T, Gou C, et al. Synergistic collaboration between regenerated cellulose and surfactant to stabilize oil/water (O/W) emulsions for enhancing oil recovery. Energy Fuel 2019;33(1):81–8. https://doi.org/10.1021/acs.energyfuels.8b02999.
[105] Anyfantakis M, Vialetto J, Best A, Auernhammer GK, Butt H-J, Binks BP, et al. Adsorption and crystallization of particles at the air-water interface induced by minute amounts of surfactant. Langmuir 2018;34(50):15526–36. https://doi.org/10.1021/acs.langmuir.8b03233.
[106] Reid MS, Erlandsson J, Wågberg L. Interfacial polymerization of cellulose nanocrystal polyamide Janus nanocomposites with controlled architectures. ACS Macro Lett 2019;8(10):1334–40. https://doi.org/10.1021/acsmacrolett.9b00692.
[107] Liu X, Shi S, Li Y, Forth J, Wang D, Russell TP. Liquid tubule formation and stabilization using cellulose nanocrystal surfactants. Angew Chem Int Ed 2017;56(41):12594–8. https://doi.org/10.1002/anie.201706839.
[108] Li Y, Liu X, Zhang Z, Zhao S, Tian G, Zheng J, et al. Adaptive structured Pickering emulsions and porous materials based on cellulose nanocrystal surfactants. Angew Chem Int Ed 2018;57(41):13560–4. https://doi.org/10.1002/anie.201808888.
[109] Wu X, Yuan Q, Liu S, Shi S, Russell TP, Wang D. Nanorod-surfactant assemblies and their interfacial behavior at liquid-liquid interfaces. ACS Macro Lett 2019;8:512–8. https://doi.org/10.1021/acsmacrolett.9b00134.
[110] V. Calabrese, M. A. da Silva, J. Schmitt, K. M. Z. Hossain, J. L. Scott, K. J. Edler, Chargedriven interfacial gelation of cellulose nanofibrils across the water/oil interface, Soft Matter (2019) https://doi.org/10.1039/C9SM01551Edoi:10.1039/C9SM01551E.
[111] Kaufman G, Mukhopadhyay S, Rokhlenko Y, Nejati S, Boltyanskiy R, Choo Y, et al. Highly stiff yet elastic microcapsules incorporating cellulose nanofibrils. Soft Matter 2017;13(15):2733–7. https://doi.org/10.1039/C7SM00092H.
[112] Tardy BL, Yokota S, Ago M, Xiang W, Kondo T, Bordes R, et al. Nanocellulosesurfactant interactions. Curr Opin Colloid Interface Sci 2017;29:57–67. https://doi.org/10.1016/j.cocis.2017.02.004.
[113] Xiang W, Preisig N, Ketola A, Tardy BL, Bai L, Ketoja JA, et al. How cellulose nanofibrils affect bulk, surface, and foam properties of anionic surfactant solutions. Biomacromolecules 2019;20(12):4361–9. https://doi.org/10.1021/acs.biomac.9b01037.
[114] Parajuli S, Dorris AL, Middleton C, Rodriguez A, Haver MO, Hammer NI, et al. Surface and interfacial interactions in dodecane/brine Pickering emulsions stabilized by the combination of cellulose nanocrystals and emulsifiers. Langmuir 2019;35(37):12061–70. https://doi.org/10.1021/acs.langmuir.9b01218.
[115] Zhang X, Liu Y, Wang Y, Luo X, Li Y, Li B, et al. Surface modification of cellulose nanofibrils with protein nanoparticles for enhancing the stabilization of O/W Pickering emulsions. Food Hydrocoll 2019;97(April):105180. https://doi.org/10.1016/j.foodhyd.2019.105180.
[116] Liu F, Zheng J, Huang CH, Tang CH, Ou SY. Pickering high internal phase emulsions stabilized by protein-covered cellulose nanocrystals. Food Hydrocoll 2018;82:96–105. https://doi.org/10.1016/j.foodhyd.2018.03.047.
[117] Sarkar A, Zhang S, Murray B, Russell JA, Boxal S. Modulating in vitro gastric digestion of emulsions using composite whey protein-cellulose nanocrystal interfaces. Colloids Surf B Biointerfaces 2017;158:137–46. https://doi.org/10.1016/j.colsurfb.2017.06.037.
[118] Hu Z, Patten T, Pelton R, Cranston ED. Synergistic stabilization of emulsions and emulsion gels with water-soluble polymers and cellulose nanocrystals. ACS Sustain Chem Eng 2015;3(5):1023–31. https://doi.org/10.1021/acssuschemeng.5b00194.
[119] Hu Z, Xu R, Cranston ED, Pelton RH. Stable aqueous foams from cellulose nanocrystals and methyl cellulose. Biomacromolecules 2016;17(12):4095–9. https://doi.org/10.1021/acs.biomac.6b01641.
[120] Bielejewska N, Hertmanowski R. Functionalization of LC molecular films with nanocrystalline cellulose: A study of the self-assembly processes and molecular stability. Colloids Surfaces B Biointerfaces (August) 2019:110634. https://doi.org/10.1016/j.colsurfb.2019.110634.
[121] Cherhal F, Cousin F, Capron I. Structural description of the interface of Pickering emulsions stabilized by cellulose nanocrystals. Biomacromolecules 2016;17(2):496–502. https://doi.org/10.1021/acs.biomac.5b01413.
[122] Bai L, Huan S, Xiang W, Rojas OJ. Pickering emulsions by combining cellulose nanofibrils and nanocrystals: phase behavior and depletion stabilization. Green Chem 2018;20(7):1571–82. https://doi.org/10.1039/C8GC00134K.

[123] Kalashnikova I, Bizot H, Bertoncini P, Cathala B, Capron I. Cellulosic nanorods of various aspect ratios for oil in water Pickering emulsions. Soft Matter 2013;9(3):952–9. https://doi.org/10.1039/C2SM26472B.
[124] Domingues AA, Pereira FV, Sierakowski MR, Rojas OJ, Petri DF. Interfacial properties of cellulose nanoparticles obtained from acid and enzymatic hydrolysis of cellulose. Cellulose 2016;23(4):2421–37. https://doi.org/10.1007/s10570-016-0965-3.
[125] Niinivaara E, Wilson BP, King AWT, Kontturi E. Parameters affecting monolayer organisation of substituted polysaccharides on solid substrates upon Langmuir-Schaefer deposition. React Funct Polym 2016;99:100–6. https://doi.org/10.1016/j.reactfunctpolym.2015.12.010.
[126] Habibi Y, Hoeger I, Kelley SS, Rojas OJ. Development of Langmuir-Schaeffer cellulose nanocrystal monolayers and their interfacial behaviors. Langmuir 2010;26(2):990–1001. https://doi.org/10.1021/la902444x.
[127] Mattos BD, Tardy BL, Rojas OJ. Accounting for substrate interactions in the measurement of the dimensions of cellulose nanofibrils. Biomacromolecules 2019;20(7):2657–65. https://doi.org/10.1021/acs.biomac.9b00432.
[128] Geisel K, Richtering W, Isa L. Highly ordered 2D microgel arrays: compression versus self-assembly. Soft Matter 2014;10(40):7968–76. https://doi.org/10.1039/c4sm01166j.
[129] Rauh A, Rey M, Barbera L, Zanini M, Karg M, Isa L. Compression of hard core-soft shell nanoparticles at liquid-liquid interfaces: inuence of the shell thickness. Soft Matter 2017;13(1):158–69. https://doi.org/10.1039/C6SM01020B.
[130] Parratt LG. Surface studies of solids by Total Reection of X-rays. Phys Rev 1954;95(2):359–69. https://doi.org/10.1103/PhysRev.95.359.
[131] Bresme F, Faraudo J. Orientational transitions of anisotropic nanoparticles at liquid-liquid interfaces. J Phys Condens Matter 2007;19:375110. https://doi.org/10.1088/0953-8984/19/37/375110.
[132] Faraudo J, Bresme F. Stability of particles adsorbed at liquid/uid interfaces: shape effects induced by line tension. J Chem Phys 2003;118(14):6518–28. https://doi.org/10.1063/1.1559728.
[133] Coertjens S, Moldenaers P, Vermant J, Isa L. Contact angles of microellipsoids at uid interfaces. Langmuir 2014;30(15):4289–300. https://doi.org/10.1021/la500888u.
[134] Reguera J, Ponomarev E, Geue T, Stellacci F, Bresme F, Moglianetti M. Contact angle and adsorption energies of nanoparticles at the air-liquid interface determined by neutron reectivity and molecular dynamics. Nanoscale 2015;7(13):5665–73. https://doi.org/10.1039/C5NR00620A.
[135] Erni P. Deformation modes of complex uid interfaces. Soft Matter 2011;7(17):7586–600. https://doi.org/10.1039/c1sm05263b.
[136] Bertsch P, Fischer P. Interfacial rheology of charged anisotropic cellulose nanocrystals at the air-water interface. Langmuir 2019;35(24):7937–43. https://doi.org/10.1021/acs.langmuir.9b00699.
[137] Bertsch P, Sánchez-Ferrer A, Bagnani M, Isabettini S, Kohlbrecher J, Mezzenga R, et al. Ion-induced formation of nanocrystalline cellulose colloidal glasses containing nematic domains. Langmuir 2019;35(11):4117–24. https://doi.org/10.1021/acs.langmuir.9b00281.
[138] Sagis LM, Fischer P. Nonlinear rheology of complex uid-uid interfaces. Curr Opin Colloid Interface Sci 2014;19(6):520–9. https://doi.org/10.1016/j.cocis.2014.09.003.
[139] Zang DY, Rio E, Delon G, Langevin D, Wei B, Binks BP. Inuence of the contact angle of silica nanoparticles at the air-water interface on the mechanical properties of the layers composed of these particles. Mol Phys 2011;109(7–10):1057–66. https://doi.org/10.1080/00268976.2010.542778.
[140] Isa L, Lucas F, Wepf R, Reimhult E. Measuring single-nanoparticle wetting properties by freeze-fracture shadow-casting cryo-scanning electron microscopy. Nat Commun 2011;2(1):438. https://doi.org/10.1038/ncomms1441.
[141] Stocco A, Su G, Nobili M, In M, Wang D. In situ assessment of the contact angles of nanoparticles adsorbed at uid interfaces by multiple angle of incidence ellipsometry. Soft Matter 2014;10(36):6999–7007. https://doi.org/10.1039/c4sm00482e.
[142] Clint JH, Taylor SE. Particle size and interparticle forces of overbased detergents: a Langmuir trough study. Colloids Surf A Physicochem Eng Asp 1992;65(1):61–7. https://doi.org/10.1016/0166-6622(92)80175-2.
[143] Aveyard R, Binks BP, Clint JH, Fletcher PD, Horozov TS, Neumann B, et al. Measurement of long-range repulsive forces between charged particles at an oil-water interface. Phys Rev Lett 2002;88(24):2461021–4. https://doi.org/10.1103/PhysRevLett.88.246102.
[144] Blaker JJ, Lee KY, Li X, Menner A, Bismarck A. Renewable nanocomposite polymer foams synthesized from Pickering emulsion templates. Green Chem 2009;11(9):1321–6. https://doi.org/10.1039/b913740h.
[145] Liu L, Kerr WL, Kong F. Characterization of lipid emulsions during in vitro digestion in the presence of three types of nanocellulose. J Colloid Interface Sci 2019;545:317–29. https://doi.org/10.1016/j.jcis.2019.03.023.
[146] Liu L, Kong F. In vitro investigation of the influence of nano-fibrillated cellulose on lipid digestion and absorption. Int J Biol Macromol 2019;139:361–6. https://doi.org/10.1016/j.ijbiomac.2019.07.189.
[147] Huan S, Ajdary R, Bai L, Klar V, Rojas OJ. Low solids emulsion gels based on nanocellulose for 3D-printing. Biomacromolecules 2019;20(2):635–44. https://doi.org/10.1021/acs.biomac.8b01224.
[148] Huan S, Mattos BD, Ajdary R, Xiang W, Bai L, Rojas OJ. Twophase emulgels for direct ink writing of skinbearing architectures. Adv Funct Mater 2019;1902990:1902990. https://doi.org/10.1002/adfm.201902990.